SANDIA REPORT

SAND96–1955 • UC–132
Unlimited Release
Printed August 1996

Characterization and Fluid Flow Simulation of Naturally Fractured Frontier Sandstone, Green River Basin, Wyoming

Hugo Harstad, Lawrence W. Teufel, John C. Lorenz, Stephen R. Brown

Prepared by
Sandia National Laboratories
Albuquerque, New Mexico 87185 and Livermore, California 94550
for the United States Department of Energy
under Contract DE-AC04-94AL85000

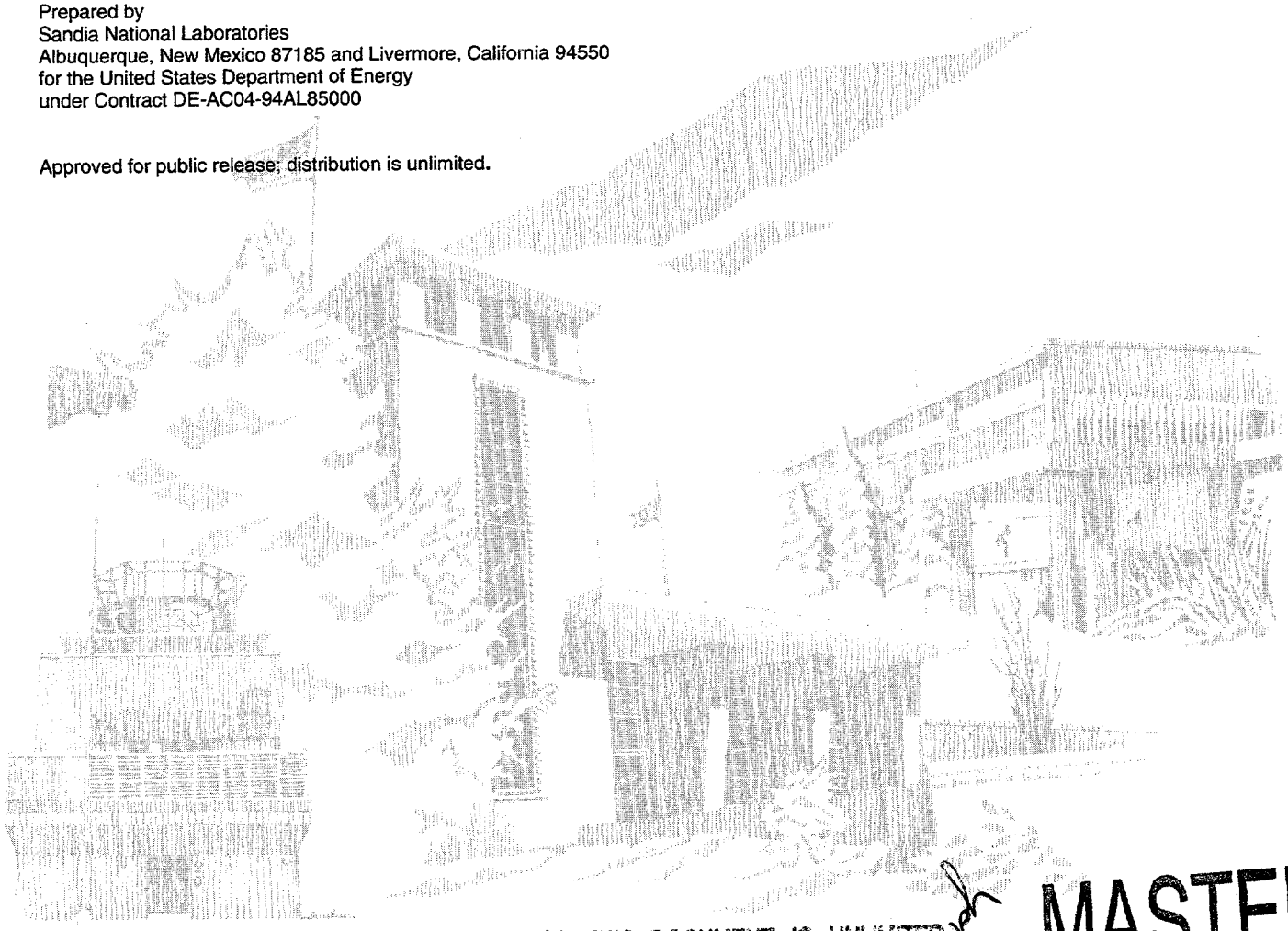

Issued by Sandia National Laboratories, operated for the United States Department of Energy by Sandia Corporation.

Available to DOE and DOE contractors from
Office of Scientific and Technical Information
PO Box 62
Oak Ridge, TN 37831

Prices available from (615) 576-8401, FTS 626-8401

Available to the public from
National Technical Information Service
US Department of Commerce
5285 Port Royal Rd
Springfield, VA 22161

NTIS price codes
Printed copy: A05
Microfiche copy: A01

SAND96-1955
Unlimited Release
Printed August 1996

Distribution
Category UC-132

Characterization and Fluid Flow Simulation of Naturally Fractured Frontier Sandstone, Green River Basin, Wyoming

Hugo Harstad
New Mexico Tech
Socorro, NM 87801

Lawrence W. Teufel*, John C. Lorenz,
and Stephen R. Brown
Geomechanics Department
Sandia National Laboratories
Albuquerque, New Mexico 87185
(*Current address: University Partnership
Regional Office at New Mexico Tech
Sandia National Laboratories
Socorro, NM 87801)

Abstract

Significant gas reserves are present in low-permeability sandstones of the Frontier Formation in the greater Green River Basin, Wyoming. Successful exploitation of these reservoirs requires an understanding of the characteristics and fluid-flow response of the regional natural fracture system that controls reservoir productivity. Fracture characteristics were obtained from outcrop studies of Frontier sandstones at locations in the basin. Fracture characterization involved construction of detailed fracture network maps of the outcrops that provided information on the fracture orientations, lengths, and spatial distribution. The fracture network maps clearly demonstrate that regional fractures are a unidirectional set of fractures that are not laterally continuous at the scale of the outcrop. The spatial distribution of regional fractures is controlled by bed thickness, with fewer and longer fractures per unit area as the bed thickness increases. The fracture data were combined with matrix permeability data to compute an anisotropic horizontal permeability tensor (magnitude and direction) corresponding to an equivalent reservoir system in the subsurface using a computational model developed by Oda (1985). This analysis shows that the maximum and minimum horizontal permeability and flow capacity are controlled by fracture intensity and decrease with increasing bed thickness. However, storage capacity is controlled by matrix porosity and

increases linearly with increasing bed thickness. The relationship between bed thickness and the calculated fluid-flow properties was used in a reservoir simulation study of vertical, hydraulically-fractured and horizontal wells and horizontal wells of different lengths in analogous naturally fractured gas reservoirs. The simulation results show that flow capacity dominates early time production, while storage capacity dominates pressure support over time for vertical wells. Thin formations have higher flow capacity but lack the necessary storage capacity and pressure support for long term production. For horizontal wells drilled perpendicular to the maximum permeability direction a high target production rate can be maintained over a longer time and have higher cumulative production than vertical wells. Longer horizontal wells are required for the same cumulative production with decreasing bed thickness.

Acknowledgment

This work was supported by Sandia National Laboratories and the U.S. Department of Energy's Morgantown Energy Technology Center. The authors thank R.L. Bruhn, University of Utah, for providing the code for calculating permeability tensors. Thanks to Phillips Petroleum Company for the use of their well performance model. Special thanks go to H.-Y. Chen for long discussions and valuable suggestions during this study.

Table of Contents

List of Tables

List of Figures

List of Abbreviations

$A^{(F)}$	anisotropy index, dimensionless
c	constant relating crack size to crack width (t = c r)
C	hydraulic conductivity, m/s
C_0	hydraulic conductivity at ground surface, m/s
E(n,r,t)	density function showing the statistical distribution of joints, dimensionless
f(r)	density function of r, dimensionless
F_0	first invariant of F_{ij}, dimensionless

F_{ij} second rank tensor for describing the geometry of joints, dimensionless

F_{ij}' deviatoric tensor of F_{ij}, dimensionless

F_n', F_m' second and third invariant of F_{ij}'

g(t) density function of t, dimensionless

H parameter controlling the change of aperture with depth, m

H(l) density function of trace lengths, dimensionless

J hydraulic gradient, dimensionless

$J^{(c)}$ hydraulic gradient along joints, dimensionless

k_{ij} permeability tensor, m^2

$\bar{k}_{ij}$ permeability tensor by numerical experiments, m^2

K directional permeability by theory, m^2

$K^{(p)}$ directional permeability by numerical experiments, m^2

$\bar{K}^{(p)}$ directional permeability best fitted to the numerical experiments, m^2

l trace length, m

L size of flow region, m

$m^{(V)}$ number of joints in volume V, dimensionless

n unit normal vector, dimensionless

N number of directions where measurements are done

$N^{(q)}/h$ number of joints intersected by unit length of a scan line with a direction q, 1/m

p unit vector parallel to the hydraulic gradient, dimensionless

P_{ij} second rank tensor describing the geometry of joints, m^2

q unit vector parallel to a scan line, dimensionless

r diameter of joint, m

t hydraulic aperture, m

T depth of flow region, m

$v^{(c)}$ seepage velocity, m/s

$\bar{v}$ apparent seepage velocity through a porous medium equivalent to a joint system, m/s

V total volume, m^3

$V^{(c)}$ volume of joints, m^3

x_1', x_2', x_3' Major, intermediate and minor principal axes

z depth below the surface, m

α gravitational acceleration, m/s^2

β rotation angle for principal axes, deg.

δ_{ij} Kronecker delta, dimensionless

ζ number of intersections per a joint, dimensionless

θ inclination angle of n to a reference axis x_1, rad.

λ geometric factor, dimensionless

ν kinematic viscosity, m^2/s

ω rotation angle for principal axes, rad.

ρ number of joints per unit volume, $1/m^3$

ϕ hydraulic head, m

$1/\psi$ mean of trace length, m

Ω solid angle corresponding to 4π, rad.

$\varnothing_f$ fracture porosity

1. Introduction

Interest in naturally fractured reservoirs has increased dramatically over the past 15 years. This has been brought about by greater industry knowledge of the effect of fractures on fluid-flow response of a reservoir and by a significant increase in oil and gas discoveries where natural fractures play a significant role in production.

Although fractures are present at some large scale in all reservoirs, it is only when they form an interconnected network with sufficient spacing and length that their effect on fluid flow becomes important. Fractures not only enhance the overall porosity and permeability of many reservoirs, but they also create significant permeability anisotropy. Knowledge of the orientation and magnitude of the horizontal permeability anisotropy has significant economic importance in developing and managing a reservoir. Such knowledge allows optimization of the location of (1) production wells for maximum primary recovery and drainage of the reservoir with the fewest number of wells, and (2) waterflood injection wells to prevent early water breakthrough in producing wells, thereby achieving maximum sweep efficiency and enhancing oil recovery.

1.1 Definition of Naturally Fractured Reservoirs

Fractures are macroscopic planar discontinuities in a rock mass that are created by deformation or diagenesis. Nelson (1982) defined a fractured reservoir as a reservoir in which naturally occurring fractures have a significant effect on reservoir fluid flow either in the form of increased reservoir permeability and/or porosity or increased permeability anisotropy. He classified fracture reservoirs into four categories based on the relative contribution of the fracture system to the overall reservoir quality:

1. Fractures provide the essential porosity and permeability.
2. Fractures provide the essential permeability.
3. Fractures assist permeability in an already producible reservoir.
4. Fractures provide no additional porosity or permeability, but create significant permeability anisotropy.

The first three reservoir types describe positive reservoir contributions of the fracture system to either the bulk reservoir permeability or effective porosity. The fourth type describes reservoirs in which fractures are important not for their contribution to reservoir quality, but how they affect reservoir permeability anisotropy and partitioning of the reservoir.

1.2 Characterization of Fracture Network

Natural fractures directly affect the bulk mechanical and fluid-flow response of a reservoir. In order to assess the role of fractures on hydrocarbon production and reservoir permeability anisotropy, characterization of naturally fractured reservoirs has focused primarily on the distribution and orientation of fractures and fluid-flow properties of individual representative fractures in a given reservoir volume (Nelson, 1982). Characterization of the fracture network can be made from analysis of cores and logs from the reservoir and surface

outcrops. Core and log studies are limited to individual fractures that intersect the wellbore and provide information on fracture orientation and distribution along the wellbore and an estimate of fracture width. These methods do not provide direct information of the spatial distribution and interconnectivity of the fracture network away from the wellbore. Analysis of fracture networks on surface outcrops that are partly analogous to the subsurface formation provide direct observation and measurement of fracture spacing, length, and interconnectivity at the scale of the outcrop exposure. An integrated approach that combines fracture information from core, log, and outcrop studies will be more successful in developing a realistic description of the subsurface fracture system in a reservoir.

1.3 Fracture Network Models

From a reservoir engineering point of view, the objective of the characterization of natural fractures is essentially to provide representative fracture permeabilities for the reservoir fluid flow study. Characterization of the fracture system must directly contribute to the fluid flow model. Unfortunately, predicting fluid-flow response of fractured reservoirs is very difficult because of the complex spatial and geometric variability of three-dimensional fracture networks. This complexity has lead petroleum engineers to characterize fracture networks with simple geometric models (Reiss, 1980). These dual-porosity models consist of matrix blocks separated by vertical, parallel fracture planes that are either a single set or two orthogonal sets of continuous parallel fractures in two or three dimensions. Permeability of the fracture network is determined primarily by the fracture spacing or size of the matrix blocks and the fracture width. Bulk reservoir permeability is determined using parallel-plate flow for the fracture network and Darcy flow for the porous matrix permeability. Reservoir permeability anisotropy occurs only if one parallel set of fractures is present or if the fracture spacing or fracture width is greater in one of the orthogonal sets of fractures.

These idealized fracture network models cannot account for variation in fracture spacing, length, orientations, and interconnectivity of the fracture system. An alternative approach to modeling fluid-flow in a fracture reservoir is to replace the fracture rock mass by an unfractured rock mass which behaves equivalently, in the sense of flow rate and pressure gradient, to the original fractured medium. This replacement can be achieved by transforming various fracture lengths, orientations, and apertures to an equivalent permeability tensor according to certain deterministic or stochastic procedures (Oda, 1985). Oda's theory is compatible with the dual-continuum concept proposed by Barenblatt (1960).

The objective of this study is to implement the computational model developed by Oda (1985) for fluid-flow response of a fractured rock mass to predict the bulk permeability of selected units of the Frontier sandstone, a naturally-fractured, tight-gas reservoir rock in Wyoming. In this study fracture characteristics obtained from outcrop studies of the Frontier sandstone at locations in the Green River Basin, Wyoming, are coupled with Oda's algorithm to determine the magnitude and direction of the equivalent permeability of an analogous subsurface naturally-fractured gas reservoir. Fracture characterization involved construction of detailed fracture network maps of the outcrops that provided information on the fracture orientations, lengths, and spatial distribution. The fracture data were then combined with

matrix permeability data to compute an anisotropic permeability tensor (magnitude and direction) corresponding to an equivalent system in the subsurface for different reservoir bed thickness. The permeability tensor was then used in a simulation study of Frontier sandstone reservoirs to predict gas production. The study included production from vertical, hydraulically-fractured wells and horizontal wells of different lengths as a function of bed thickness.

2. Geology of the Frontier Formation in the Green River Basin, Wyoming

In the Upper Cretaceous period, the Green River Basin of southwestern Wyoming was part of a narrow seaway that extended from the Gulf Coast to the arctic (Figure 2.1). During this time several thousand feet of sediment were deposited. Uplifted areas west of Wyoming provided large volumes of clastics of mainly fine, medium, and coarse sand that were transported eastward in fluvial, littoral, and marine environments. Large volumes of silt and clay were also derived from the west highlands, and were transported eastward to lower-energy marine environments that extended past the higher-energy environments (Barlow *et al.*, 1993).

The Green River Basin is bounded to the south by the Uinta Mountains uplift, to the east by the Rock Springs Uplift, to the north by the Wind River Range, and the Sevier thrust belt to the west (Figure 2.2). Today major oil and gas reserves are associated with the Upper Cretaceous deposits in the basin, particularly the Frontier Formation.

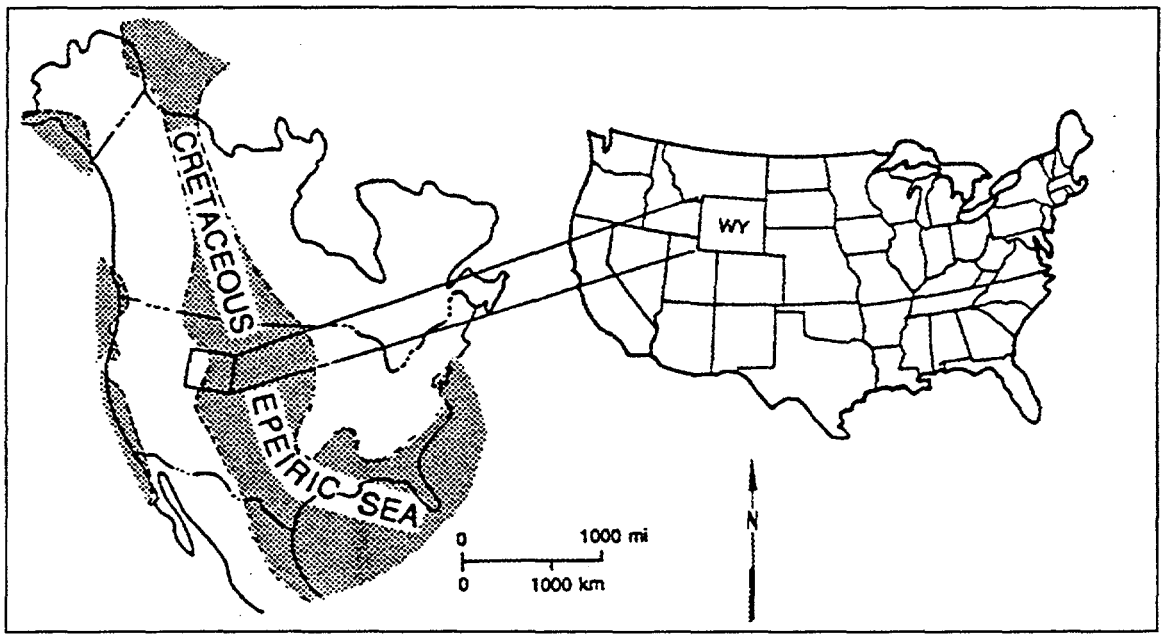

Figure 2.1. Paleogeographic reconstruction of the Western Interior Cretaceous seaway. The narrow seaway extended from the Gulf Coast to the arctic. Adapted from Moslow and Tillman, 1989.

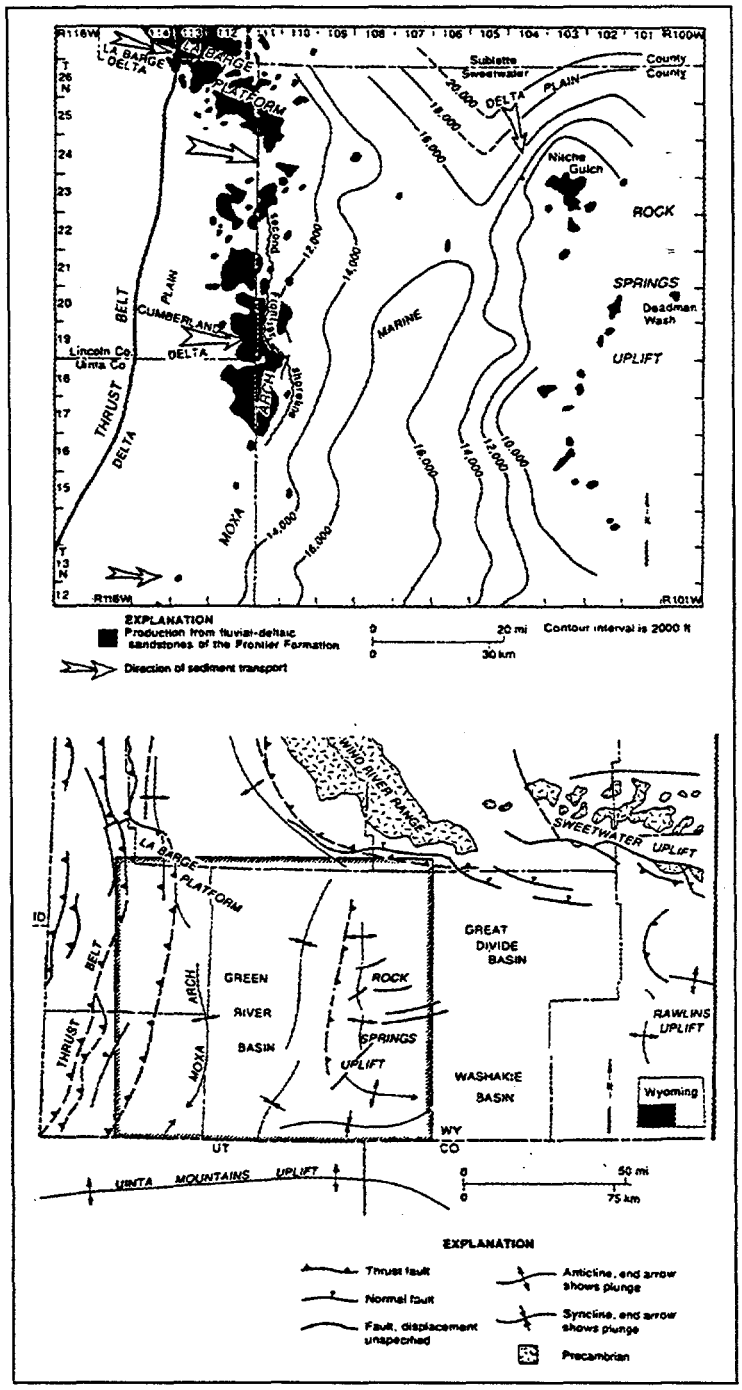

Figure 2.2. Map showing the Frontier Formation fluvial-deltaic sandstone subplay in the Green River Basin, of southwest Wyoming with major tectonic features. Both the first and second Frontier sandstones are productive in the fluvial-deltaic sandstone subplay, although the first Frontier is limited to the La Barge platform area. Adapted from Barlow et al., 1993.

2.1 Geologic Description of Frontier Formation

The Frontier Formation was named by Knight (1902) for exposures north of Frontier, a small coal mining community near Kemmerer, on the west edge of the Green River Basin of Wyoming. Veatch (1906, 1907), dated the Frontier as Colorado in age, corresponding to the early part of the Late Cretaceous. The Frontier Formation is a sequence of marine, deltaic, and fluvial sandstones interbedded with shales and is present over most of Wyoming. The formation is a stratigraphically complex exploration target with multiple stacked reservoirs, reflecting changes in eustatic sea level, variability in sediment supply, and a high degree of tectonism. Excellent outcrops of the Frontier Formation occur on the margins of the basin and provide the basis for reconstruction of the complex geologic history of deposition.

The Frontier Formation consists of two progradational fluvio-deltaic sequences separated by a transgressive marine shale. The evidence for this interpretation is based on primary sedimentary structures, fossil and tracefossil assemblages, lateral and vertical lithologic changes, and intertonguing relationships of adjacent rock types (Myers, 1977).

As shown in Figure 2.4 the Frontier Formation is overlain by Hilliard Shale and underlain by the Mowry Shale, a siliceous marine shale and source rock (Doelger et al., 1993). In westernmost Wyoming, the Frontier Formation is subdivided into five members that are, from youngest to oldest, the Dry Hollow, Oyster Ridge Sandstone, Allen Hollow, Coalville, and Chalk Creek Members. The members are fluvial-dominated clastic wedges deposited during low-strand sea level. The major productive sandstones on the Moxa arch and La Barge platform are equivalent to the Dry Hollow and Oyster Ridge Sandstone Members. At times, sediment supply was greater than the rate of subsidence, and coarse clastics derived from the west, spread eastward from the area of the present-day Thrust Belt of western Wyoming. The dominant sediments in this region are deltaic deposits of the Cumberland Delta, derived from the west, in central part of the Moxa arch (De Chadenedes, 1975, Mullen 1993) and deltaic deposits, derived from the north and northwest, on the La Barge platform and the north Rock Springs uplift (Figure 2.3).

Thickness of the Frontier Formation ranges from approximately 610 to 792 meters (2,000 to 2,600 feet) (Obradovich and Cobban, 1975). Each sandstone sequence is generally capped by impermeable, carbonaceous, delta-plain mudstones and silty shales (Figure 2.4). Core analysis from wells in the Whiskey Buttes area suggests that the lack of production to the east of the arch axis is related, at least in part, to the absence of delta-plain mudstones (bay, marsh, abandoned-channel facies) serving as stratigraphic seals for the underlying channel and shoreface reservoir facies (Moslow and Tillman, 1989).

The best quality reservoirs of the second Frontier are developed in the channel sandstones of the first bench and the uppermost shoreface and foreshore sandstones of the second bench (Figure 2.5, Moslow and Tillman, 1984).

Marine reservoirs dominate production to the north on the Moxa arch and fluvial reservoirs are dominant to the south. Porosity and permeability are low, and most of the area

of second Frontier production was designated as a tight formation (less than 0.1 md permeability) in 1980 and 1981 (Mullen, 1993).

The first Frontier sandstone, subsurface destination or Oyster Ridge sandstone outcrop is the most prolific producer on the Dry Piney structure. However, most of the reserves in the field are contained in the second Frontier (De Chadenedes, 1975). West of the Darby or Hogsback thrust, accumulation in the Frontier is essentially structurally controlled. East of the thrust, accumulation is both structurally and stratigraphically controlled (De Chadenedes, 1975).

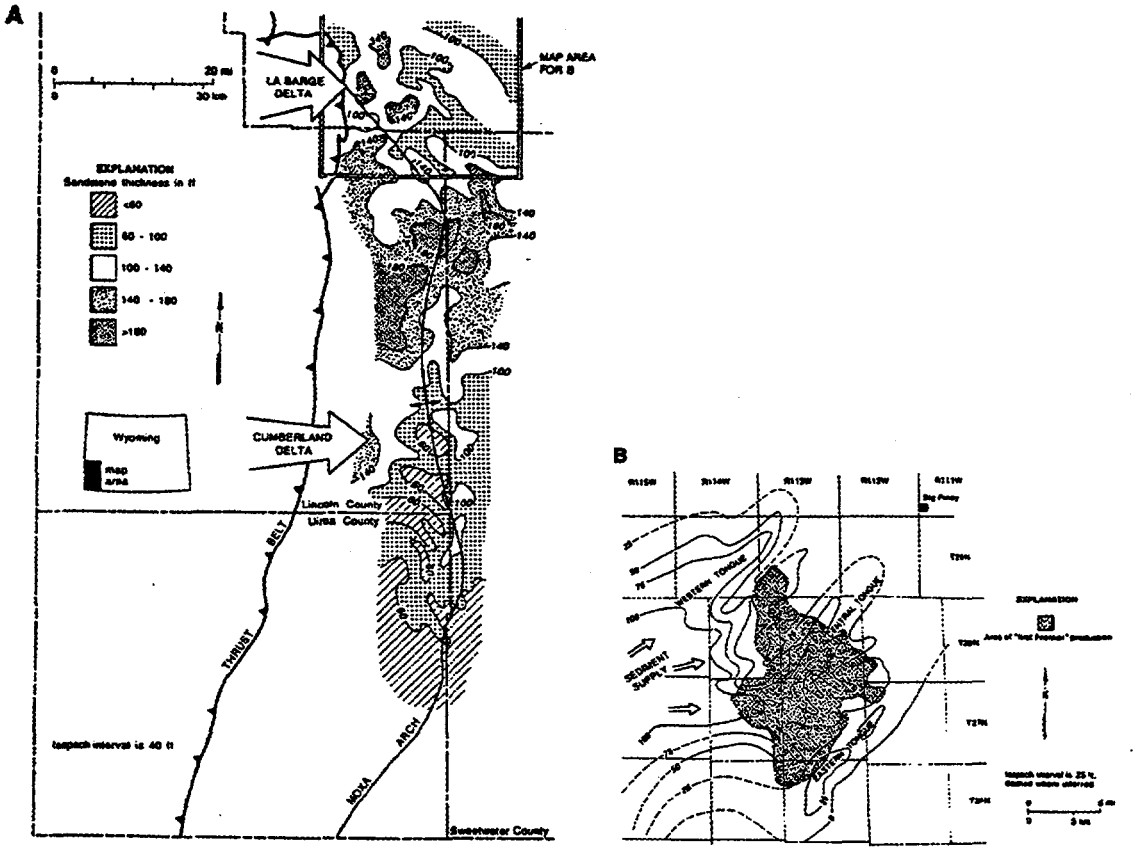

Figure 2.3. Isopach maps showing distribution of Frontier Formation. A: Second Frontier sandstone (all benches combined) along the Moxa arch and La Barge platform, from Hamlin, 1991. B: First Frontier sandstone at La Barge and the productive area. Sediment source direction is based on outcrop and subsurface studies. From Myers, 1977.

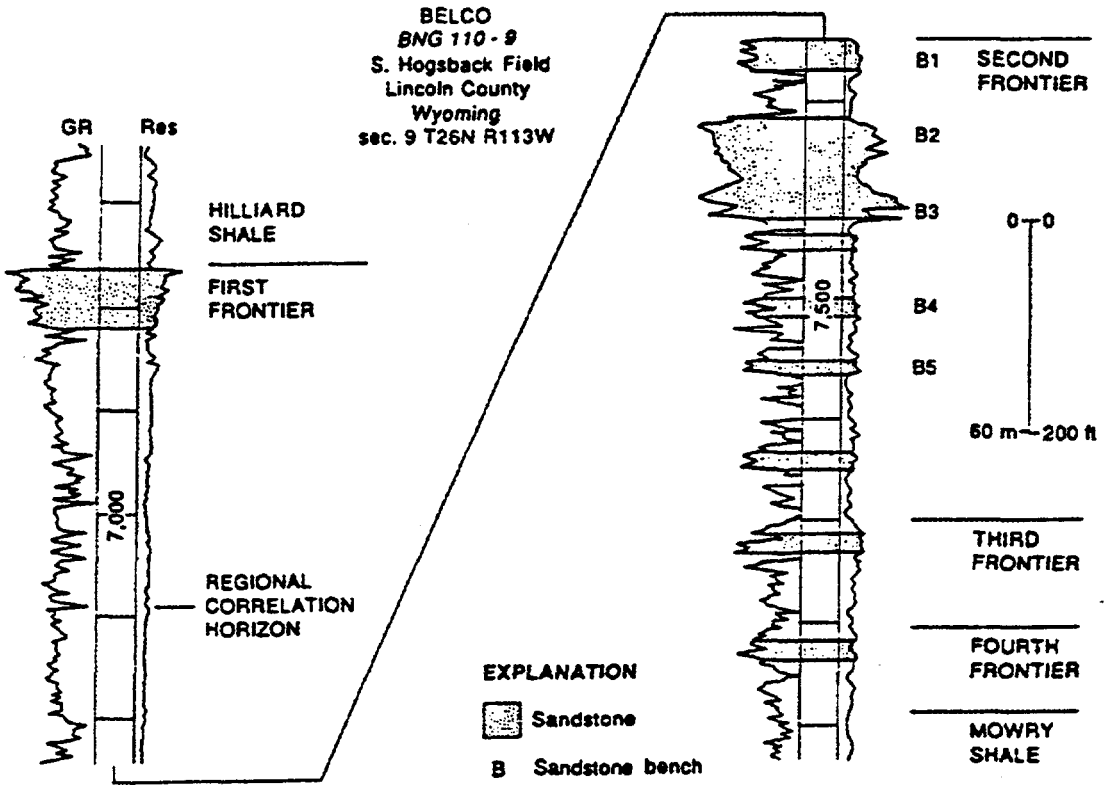

Figure 2.4. Typical gamma-ray/resistivity log of the Frontier Formation in north Moxa arch area. Showing vertical distribution of Frontier sandstones (shaded). Note the correlation marker, which is used throughout the western Green River Basin. Adapted from Dutton and Hamlin, 1991.

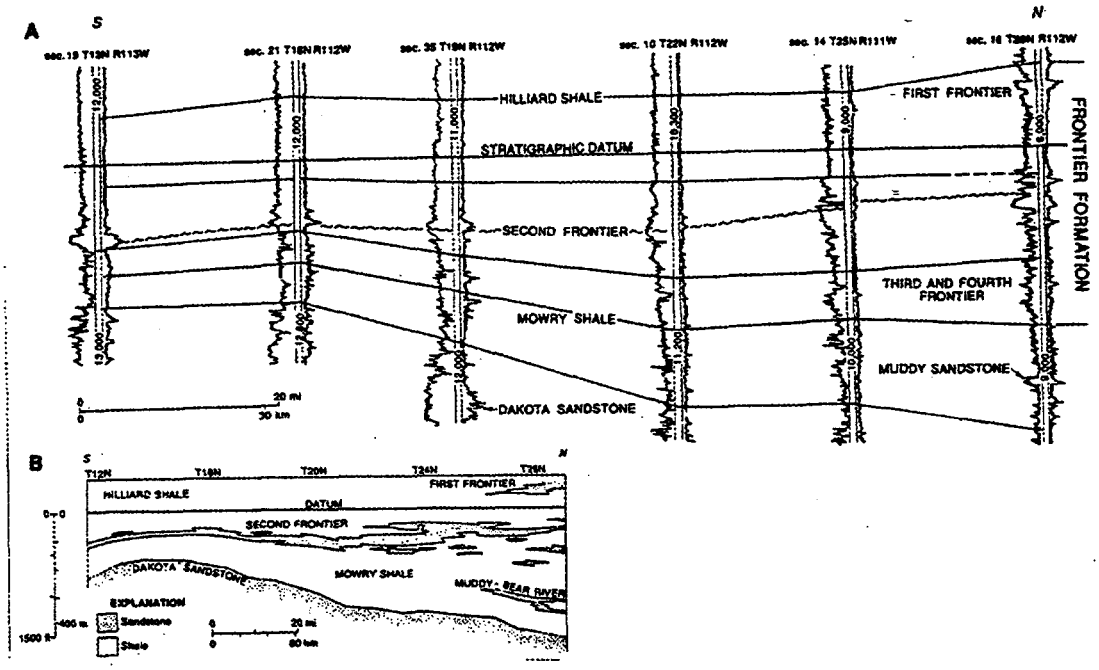

Figure 2.5. Cross section of the Frontier Formation along the Moxa arch, western Green River Basin. A: Gamma-ray/resistivity logs showing an erosional unconformity (dashed wavy lane) in the second Frontier that separates the first bench fluvial channel-fill sandstone from the underlying second bench marine shoreline sandstone. Other (solid) lines are correlations based on chronostratigraphic horizons. Formation boundaries are not shown. Adapted from Dutton and Hamlin, 1992. B: Diagrammatic section along the same line as A: showing generalized sandstone distribution in the Frontier Formation. Adapted from Dutton and Hamlin, 1991

2.2 Tectonics and Natural Fractures

The Frontier Formation has been subjected to several horizontal tectonic stress events, the most obvious event being the eastward-directed thrusting of the Sevier fold and thrust belt. Some of the tectonic events created stresses that led to regional fracturing in the sandstones. In addition, regional tectonism produced local structures, and the resulting stresses created local fractures sets within the thrust belt (Lorenz, 1995).

Fractures enhance reservoir quality in more tectonically active areas and are also likely to provide pathways for hydrocarbon migration from the underlying Mowry Shale source rock (Doelger *et al.*, 1993). Moslow and Tillman (1989) stated, from their study of the Moxa area, that there appeared to be no correlation between the thickness of these reservoir facies and the net production. The reason is probably due to the fracture network that controls the production, and that thinner zones are more intensely fractured.

2.3 Gas Production from the Frontier Formation

Estimates of Gas-In-Place range between 2,000 TCF (The Scotia Group, 1993) and 5,000 TCF (Law *et al.*, 1989) for the Greater Green River Basin. A significant proportion of that gas is found in the Frontier Formation, one of the best documented and developed examples of fluvial-deltaic sandstone gas reservoirs. More than 94% (1,875 TCF) of the gas is from reservoirs on the Moxa arch and La Barge platform of the western Green River Basin. The remaining 6% (119 BCF) is from Nitchie Gulch and Deadman Wash Frontier reservoirs at the north end of the Rock Springs uplift.

A major portion of Frontier oil and gas production is from the greater La Barge field. The field is a combination of stratigraphic and structural traps. Gas production can be from any Frontier sandstone interval and wells commonly produce from several intervals simultaneously. Sustained gas flow may be as high as 16,000 MSCFD (Petroleum Information, 1976). Condensate is also produced from various intervals, but only in small quantities. Along the Moxa Arch the sustained production averages between 1,000 and 2,000 MSCFD, and has initial potential of up to 4.3 MSCFD (Myers, 1977).

Field development for the gas reservoirs in the Frontier Formation was originally on 640-acre spacing, but in the past few years well density has increased with selective in-fill drilling. Production has remained relatively constant. Stratigraphic cross sections reflect minimal communication between distributary channel sandstone bodies. The channel sandstones are interpreted to be a series of individual isolated reservoirs and communication between channel sandstone bodies on a 360 acre per well drilling density is probably minimal. Hydraulic fracturing has been critical to connecting sufficient permeabilities and porosities in these reservoirs for economical production (Moslow and Tillman, 1989).

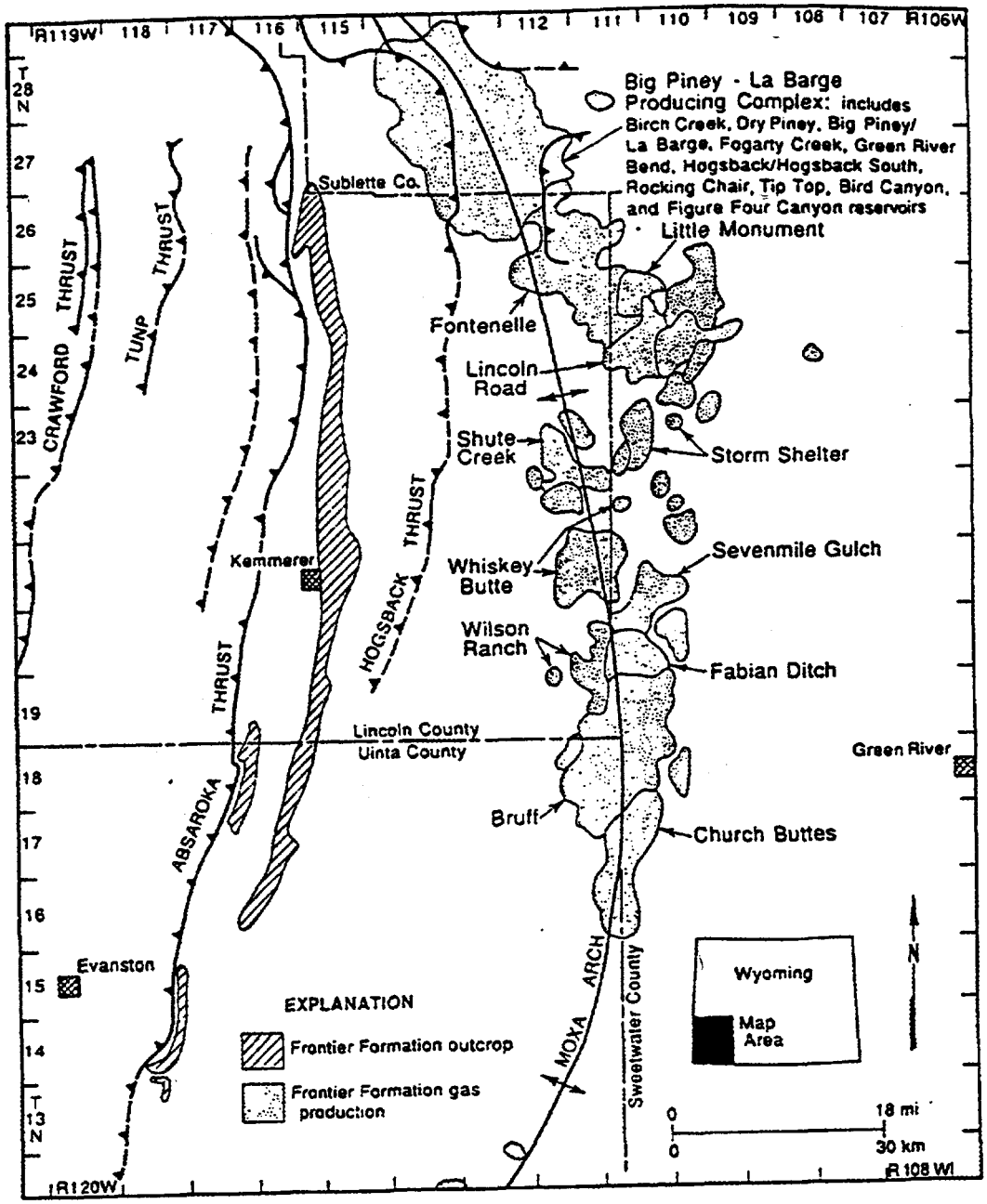

Figure 2.6. Frontier formation gas production from the Moxa Arch and La Barge platform in west Green River Basin. Frontier formation outcrops in the Thrust Belt are also shown. There are more than 25 field names for producing areas on the Moxa arch and La Barge platform, but field boundaries are often defined by lease ownership and unitized areas rather than geologic changes. Reservoirs with >5 BCF cumulative production through December 1990 are labeled. Barlow & Haun, Inc. file maps.

3. Regional Fractures

Regional fractures are systematic fractures that are developed over large areas of sedimentary basins. In general, regional fractures have relatively little change in orientation, show no evidence of offset, and are perpendicular to bedding (Stearns and Friedman, 1972). Regional fractures are pervasive in the Frontier Formation and directly influence gas productivity.

3.1 Characteristics of Regional Fractures

Regional fractures are common in relatively undeformed, flat-lying strata at the surface and in the subsurface. At the surface regional fractures commonly occur as two orthogonal sets, both oriented perpendicular to bedding (Stearns and Friedman, 1972; Kulander *et al.*, 1979). Fractures of the older set are generally laterally extensive and parallel to subparallel, whereas fractures of the younger, cross-fracture set are typically shorter, less planer, less regular in orientation, and commonly terminate against fractures of the older set. Several studies have shown that the cross fractures at the surface may be a result of stress relief during uplift and unloading and may not be present in the subsurface (i.e. Nickelsen and Hough, 1967; Lorenz and Finley, 1991). Core analysis of regional fractures in sandstones of the Mesaverde formation supports this conclusion and indicates that only one unidirectional set of regional fractures may be present in a subsurface reservoir (Lorenz et al., 1991).

3.2 Influence of Lithology and Bed Thickness

Several studies have shown that regional fractures occur in almost any lithologies from granodiorites (Segall and Pollard, 1983) to sandstones and limestones (Hancock *et al.*, 1984) to shales (Parker, 1942 and Kulander *et al.*, 1979). In general, these fractures are often limited to, or are more abundant in the more brittle lithologies in a stratigraphic sequence (e.g. Mallory, 1977), and fracture terminations often occur at bedding contacts with more ductile lithologies. Lorenz *et al.* (1991) observed vertical, regional fractures in Mesaverde sandstone abruptly terminating at the interface of bounding shale layers.

Spacing of regional fractures is influenced by bed thickness. In general, thinner beds have more closely spaced fractures (Harris *et al.*, 1960; Hodgson, 1961), and spacing is commonly less than the bed thickness. A linear relationship between fracture spacing and bed thickness has been demonstrated for specific outcrops of evenly bedded lithologies (e.g. Bogdonov, 1947; Verbeek and Grout, 1984; Angelier *et al.*, 1989). However, this relationship deteriorates rapidly for beds greater than about 0.5 m thick (Ladeira and Price, 1981). The spacing and distribution of fractures in heterogeneous beds can be very irregular, being a function of the irregular mechanical bedding units created by sedimentary heterogeneities (Lorenz *et al.*, 1989 and Lorenz and Hill, 1991). Consequently, fracture lengths, orientations, and spacing will vary laterally and the fractures tend to be en-echelon (Figure 3.1).

3.3 Origin of Regional Fractures

Several theories have been proposed for the origin of regional fractures. Price (1959) suggested that the shortening and subsequent lengthening of strata as they subsided to and then below a chord of the earth's surface during burial in a sedimentary basin could cause fracturing. Pollard and Aydin (1988) and others have suggested that regional fractures are natural hydraulic fractures that develop when the pore pressure locally exceeds the tensile strength of the rock. Both mechanisms may create fractures locally, but cannot account for the widespread and consistent patterns of regional fractures.

Lorenz *et al.* (1991) proposed that regional fractures are extension fractures that form during far-field compression, initiate at locally induced tensile stresses caused by flaws in the rock, and propagate in the plane of the maximum and intermediate principal compressive stresses (Figure 3.1). The differential stress required for initiation and propagation of regional fractures is well below that necessary for shear failure. In the presence of high pore pressure, fractures can be held open at depth by a tectonic, basinwide dilatancy of the strata, and the open void space commonly becomes mineralized.

3.4 Influence of Regional Fractures on Reservoir Permeability

Regional fractures have great economic significance, since they may enhance or, if tightly mineralized, obstruct permeability in any formation in which they are found (Lorenz and Finley, 1989). In either case, unidirectional regional fractures can create highly anisotropic horizontal permeability in a reservoir. Elkins and Skov (1960) reported reservoir permeability anisotropy of 1000 to 1 in an oil field in the Spraberry trend in west Texas. Lorenz et al. (1989) measured a permeability anisotropy of more than 100 to 1 in tight-gas reservoirs of the Mesaverde formation in the Rulison field, Colorado. In both these cases the matrix rock is tight and fluid-flow in the reservoir is dominated by unidirectional regional fractures.

Regional fracture systems produce oil and gas in numerous fields including Big Sandy field in Kentucky and West Virginia, Spraberry Trend in west Texas, Altamount-Blue Bell field in Utah, and the Rulison field in Colorado. High-quality fractured reservoirs occur when tectonic fracture systems associated with structural traps are superimposed on a regional fracture trend. Regional fractures are of particular importance in stratigraphic traps in low-permeability gas reservoirs, such as the Frontier formation of Wyoming, because they provide the essential reservoir permeability.

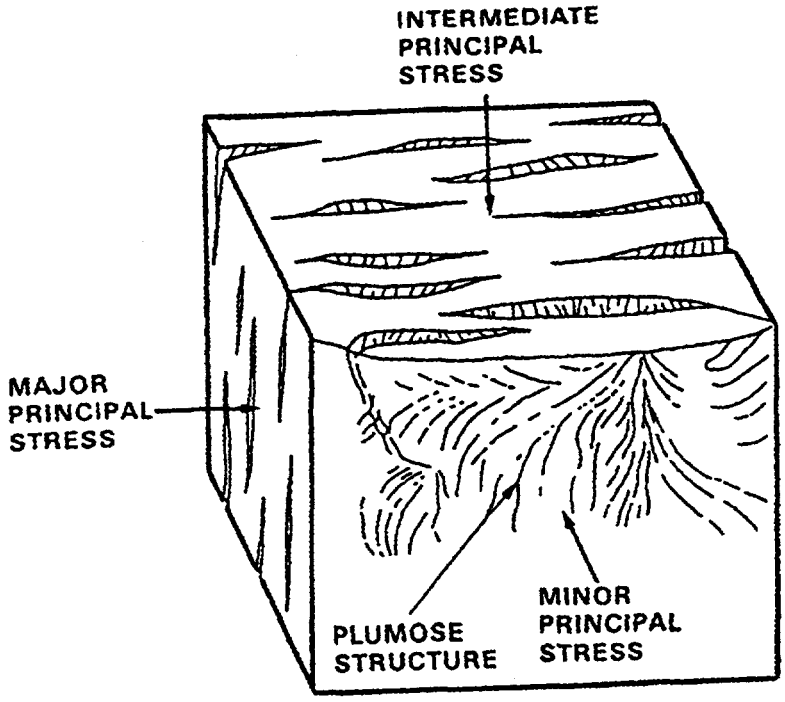

Figure 3.1. Schematic representation of regional fractures in outcrop. From Gramberg, 1965. Note that the major and intermediate principal stresses can be exchanged without altering fracture orientation.

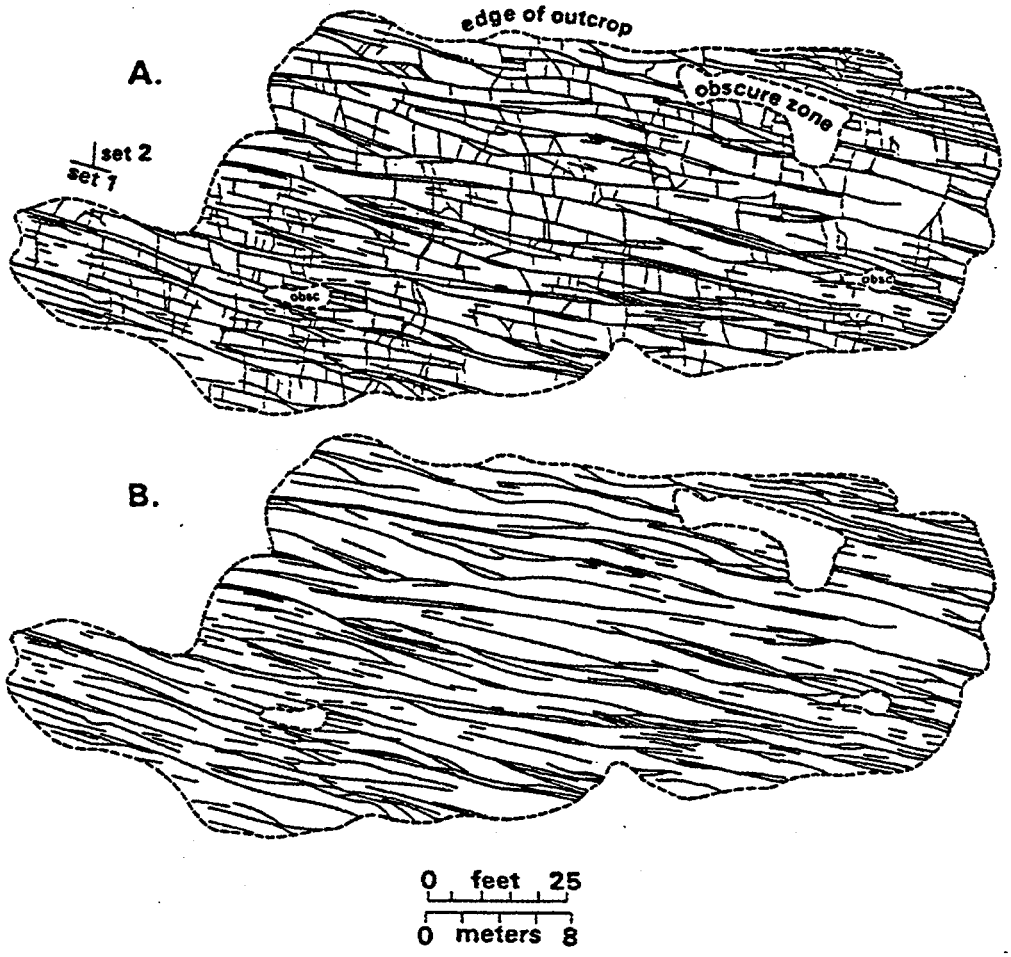

Figure 3.2. Plan view of regional fracture patterns in a sandstone bed of the Mesaverde Formation at Rifle Gap. A, all fractures, B dominant fracture set only. From Lorenz and Finley, 1991.

4. Fracture Characterization Of Frontier Sandstone Outcrops

Characterization of natural fracture systems can be made from the analysis of cores and logs in the subsurface and from surface outcrops. In this study fracture characterization of the Frontier sandstone will focus only on analysis of surface outcrops, because this approach provides the spatial distribution and interconnectivity of the fracture network which is essential to calculate the bulk permeability. The outcrop fracture data will be combined with matrix permeability data to compute an anisotropic permeability tensor of a system equivalent to a Frontier sandstone gas reservoir in the subsurface.

Surface exposures of the Frontier formation are present along the edge of the Green River Basin. Four outcrops of sandstones in the Frontier formation with different bed thickness were selected for this study based on an aerial survey of the basin and preliminary field investigations. Each of the outcrops are large well-exposed pavements of sandstone bedding planes that contain a well-developed natural fracture network. Fractures are perpendicular to bedding and make these surface pavements ideal for mapping the orientation, length and spatial distribution of natural fractures along the bedding plane.

Figure 4.1 shows outcrop locations. Locations of two of the outcrops are on the southwestern edge of the basin 33 km (20.5 miles) and 39 km (24 miles) south of Kemmerer, Wyoming along the Hogsback escarpment, which is an expression of the Hogsback thrust plate, which is part of the Idaho-Wyoming thrust belt. The first outcrop was at Scullys Gap and the second outcrop was at Bridger Gap. The third outcrop is at the state border, 2 km east of Flaming Gorge Reservoir, Wyoming, and is on the north flank of the Uinta Mountains uplift. The fourth outcrop is at Muddy Gap, 110 km (70 miles) north of Rawlins, Wyoming, on US. Highway 287.

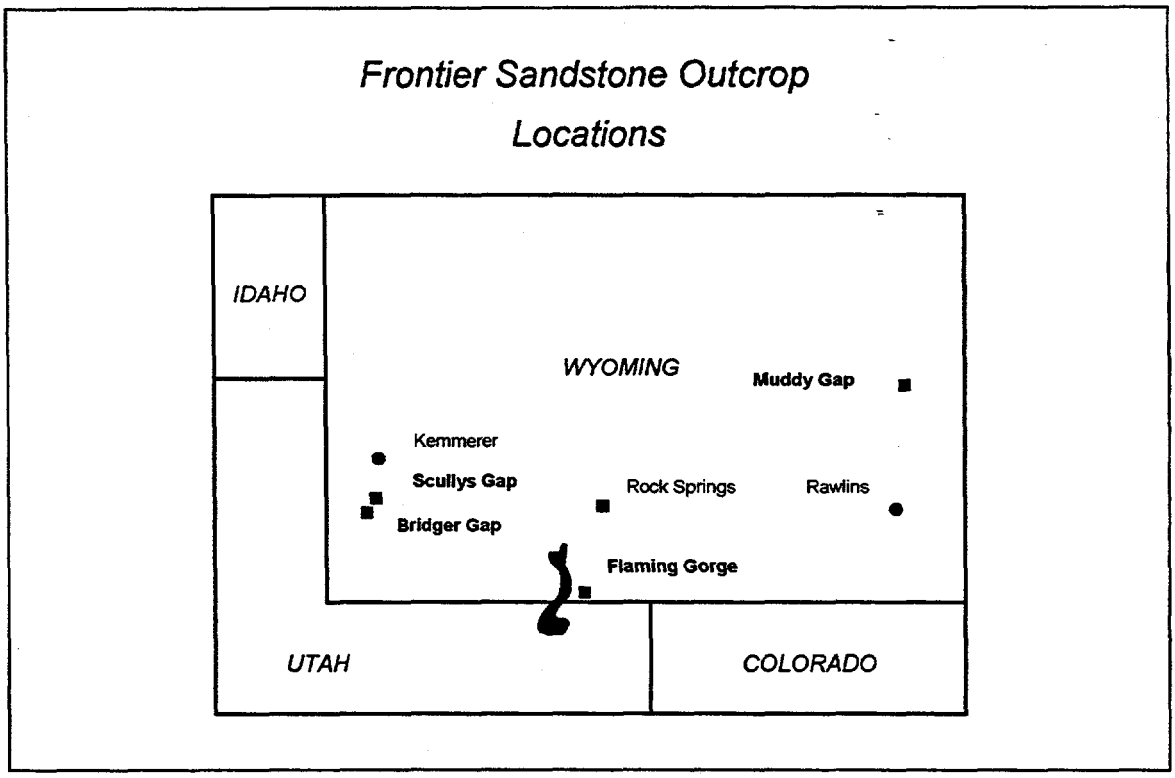

Figure 4.1. Map of Southwestern Wyoming. Surface exposures of the Frontier Formation are present along the margins of the Green River Basin. The locations of the Frontier Sandstone outcrops used in the fracture characterization study is marked with squares.

4.1 Fracture Mapping Procedures

Regional extension fractures are well-exposed at each outcrop and are the dominant fracture set. The regional fractures are clearly visible on aerial photos of the bedding plane surface (Figure 4.2).

At each outcrop detailed maps of a representative fracture network were constructed. To map the fracture networks a rectangular grid was laid out on the surface pavement using a series of measuring tapes. The orientation of the grid was placed so that one side of the grid was parallel to the dominant regional fracture trend. The size of the grid was determined by the average fracture spacing and was of sufficient size to obtain a representative spatial distribution of the fracture network. The grids ranged in size from 18.3 m (60 ft) by 4.3 m (14 ft) at Scullys Gap where the average fracture spacing is less than 0.5 m, to a grid that was 317 m (1040 ft) by 60 m (197 ft) at Muddy Gap where the average fracture spacing was greater than 10 m. The orientation of each grid was referenced to true north and the strike and dip of each outcrop bedding plane was also measured.

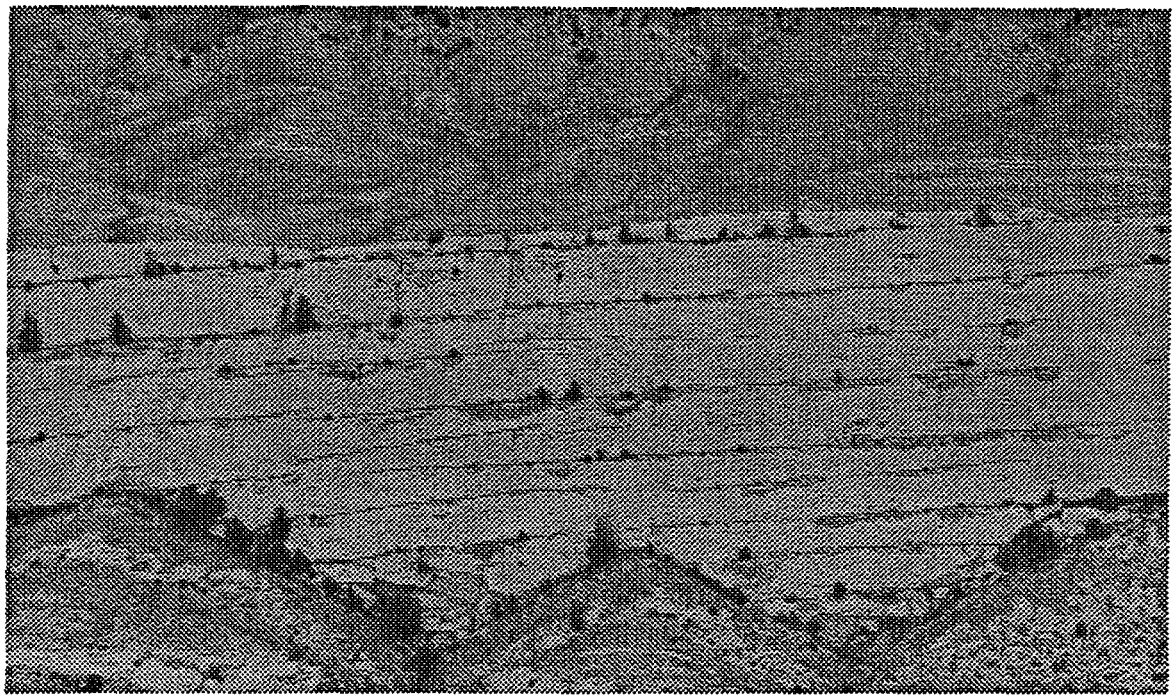

Figure 4.2 Aerial photo showing regional fractures on the outcrop at Muddy Gap, 110 km north of Rawlins on US Highway 287. The regional fracture network at this outcrop is a well-developed subparallel fracture set, but the fractures are not always continuous.

The orientation and length of each fracture in the grid was mapped by walking out each fracture and tracing the fracture trend and position onto a grid block map. The morphology of the fractures were described as open or filled, and whether the fracture was en echelon with respect to adjacent fractures or not. The nature of the termination of each fracture was also noted.

The fracture maps provide information on the spatial distribution of the fracture system in two-dimensions at the bedding plane surface. Vertical continuity of the fractures through the sandstone bed was examined at the edge of each outcrop. Average bed thickness was measured at each outcrop in order to determine the influence of bed thickness on fracture intensity.

4.2 Fracture Maps

The fracture map from Scullys gap is shown in Figure 4.3. More than one set of fractures is present, reflecting fractures that are related to regional and local tectonics, as well as fractures that are associated with stress relief during uplift and erosion. Regional fractures are the longest fractures. The azimuth of the regional fracture trend is N19°E. The edge of the outcrop parallels the regional fracture trend. Bed thickness of the sandstone layer at this outcrop is 0.2 m. Fractures observed at the edge of the outcrop are perpendicular to bedding, show vertical continuity through the bed, and terminate at the underlying shale layer.

Figure 4.4 shows the fracture network map at Bridger Gap, south of Kemmerer. The dominant set of subparallel fractures is the regional fracture trend. The azimuth of the regional fractures is N13°E. This orientation is consistent with regional fracture azimuth at Scullys Gap which is located 6 km north of this outcrop. Note that many of the regional fractures are not continuous at the scale of the outcrop and do not have equal spacing. Fracture length is also not constant and in many cases the fractures are en echelon. Bed thickness of this sandstone layer is 2 m. Fractures observed at the edge of the outcrop are perpendicular to bedding and vertically continuous through the sandstone bed.

The fracture network map of the outcrop east of Flaming gorge is shown in Figure 4.5. A unidirectional regional fracture system is well developed at this location. The azimuth of the regional fracture trend is N39°W. The regional fractures again are not continuous through-going fractures and do not have equal spacing. Fracture length ranges from less than one meter to about 28 m. Estimated bed thickness is three meters. Fractures at this outcrop are also vertically continuous through the sandstone bed.

Figure 4.6 shows the fracture network map at Muddy Gap. The regional fracture network at this outcrop is a well-developed subparallel fracture set. The azimuth of the regional fracture trend is N44°W. Fracture length and spacing is the greatest of the four outcrops studied. The longest fracture is nearly 300 m in length. The estimated bed thickness is also the greatest of the four outcrops and is about 6 m. Fractures at this outcrop are also vertically continuous through the sandstone bed and terminate at the underlying shale. A fracture subset at the upper left corner of the map is believed to be the result of weathering and edge effects.

Vertical continuity of the regional extension fractures, through the sandstone bed was examined at the edge of each outcrop and shows that the fractures crossed the entire bed thickness and terminated at the underlying shale layer.

In general, the four fracture network maps clearly show that regional fractures are not laterally continuous at the scale of the outcrop and are certainly not continuous for analogous bed thicknesses at the reservoir scale. Fewer fractures occur per unit area as the bedding thickness increases, however fractures do not have a consistent and equal spacing for a given bed thickness. The length of a regional fracture is highly variable and tends to increase with bed thickness. In many cases the outcrop fracture maps show the fractures to be en echelon, forming small local fracture swarms.

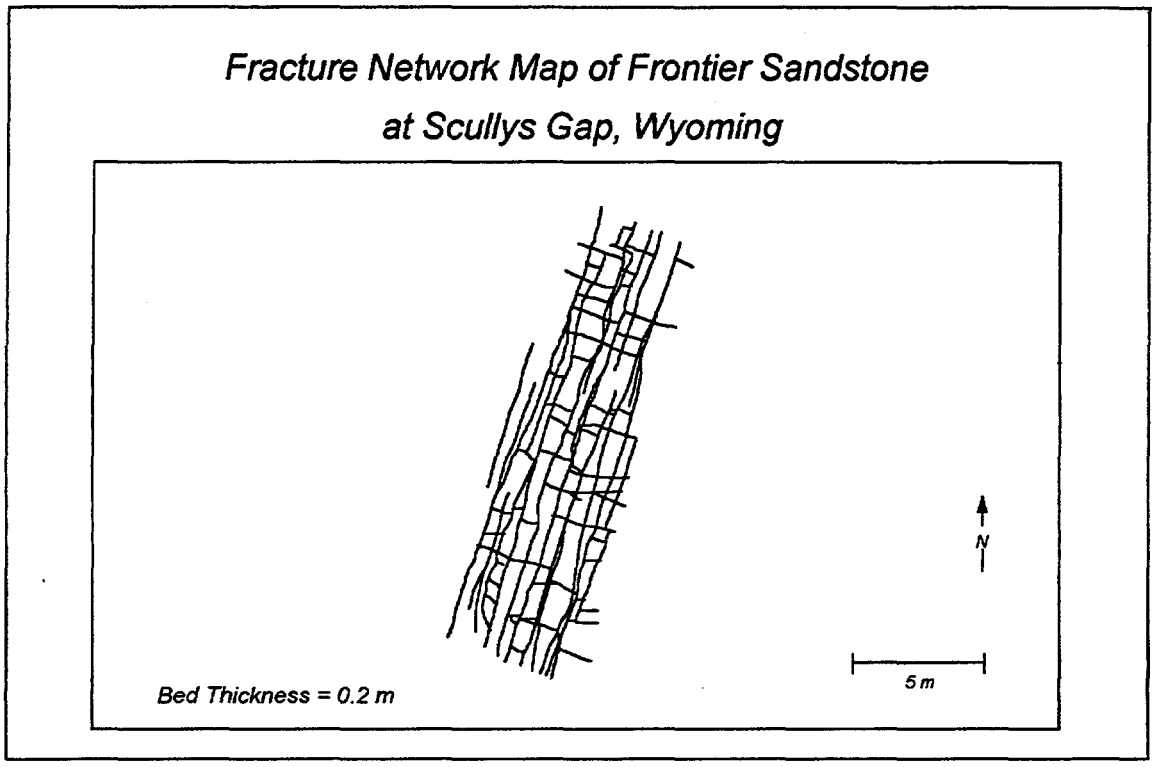

Figure 4.3. Fracture network map made of the outcrop at Scullys Gap, 33 km South of Kemmerer, Wyoming. More than one set of fractures is present, reflecting fractures that are related to regional and local tectonics, as well as fractures that are associated with weathering. Regional fractures are the longest fractures. The azimuth of the regional fracture trend is N19°E. Bed thickness of the sandstone layer at this outcrop is 0.2 m.

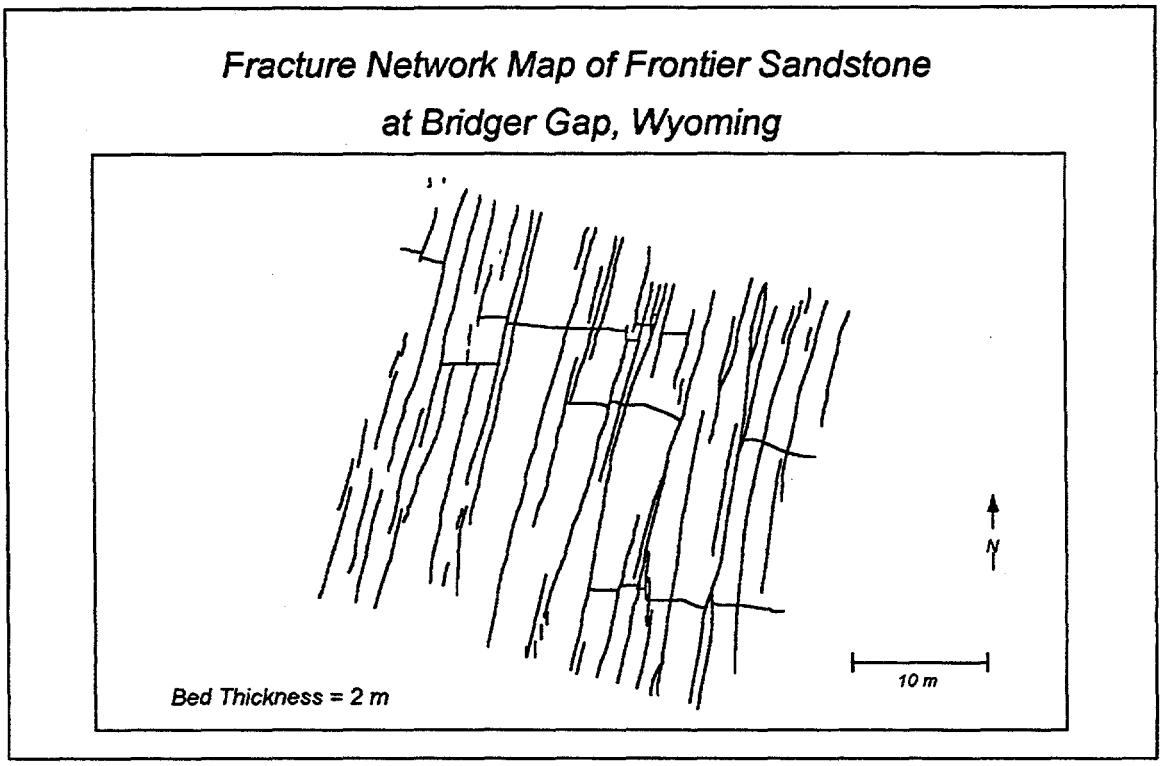

Figure 4.4. Fracture network map of the outcrop at Bridger Gap, 39 km south of Kemmerer, Wyoming. The dominant set of subparallel fractures is the regional fracture trend. Note that many of the regional fractures are not continuous at the scale of the outcrop and do not have equal spacing. Fracture length is also not constant and in many cases the fractures are en echelon. The azimuth of the regional fractures is N13°E. This orientation is consistent with regional fracture azimuth at Scullys Gap (Figure 4.3) which is located 6 km north of this outcrop. Bed thickness of this sandstone layer is 2 m.

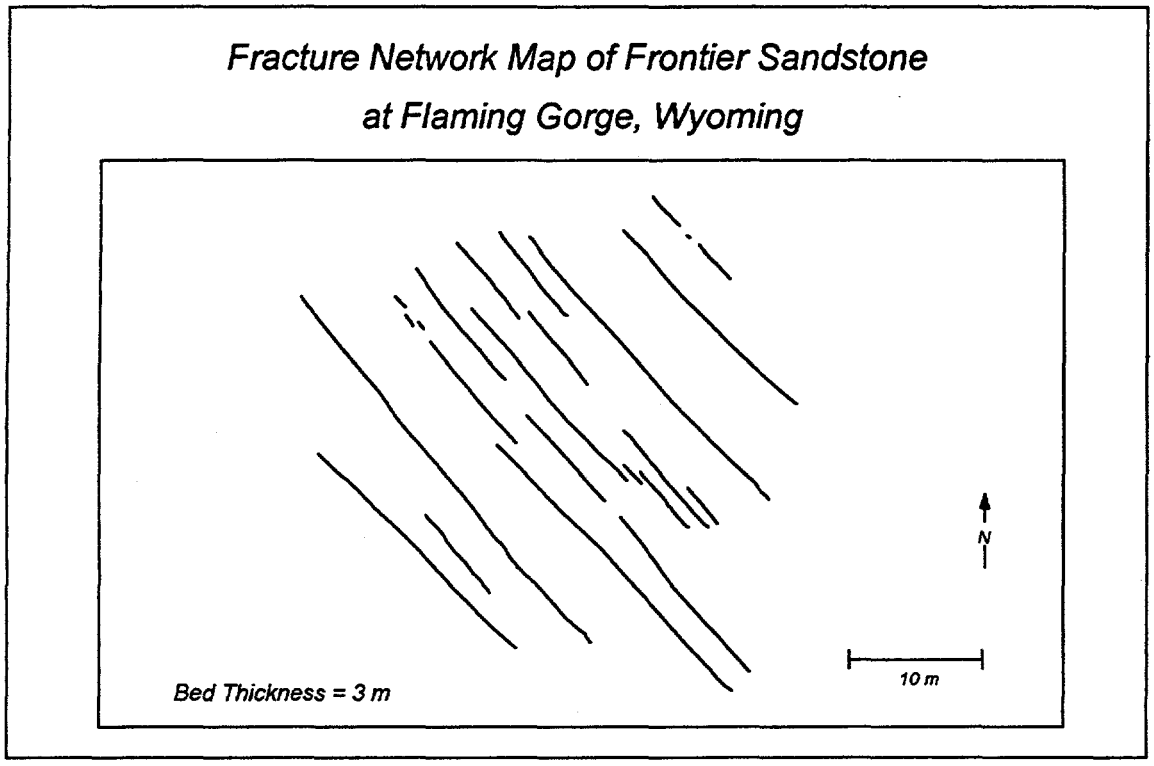

Figure 4.5. Fracture network map made of the outcrop 2 km east of Flaming Gorge, Wyoming on the north flank of the Uinta Mountains uplift. A unidirectional regional fracture system is well developed at this location. The regional fractures again are not continuous through-going fractures and do not have equal spacing. The azimuth of the regional fracture trend is N39°W. Estimated bed thickness is 3 m.

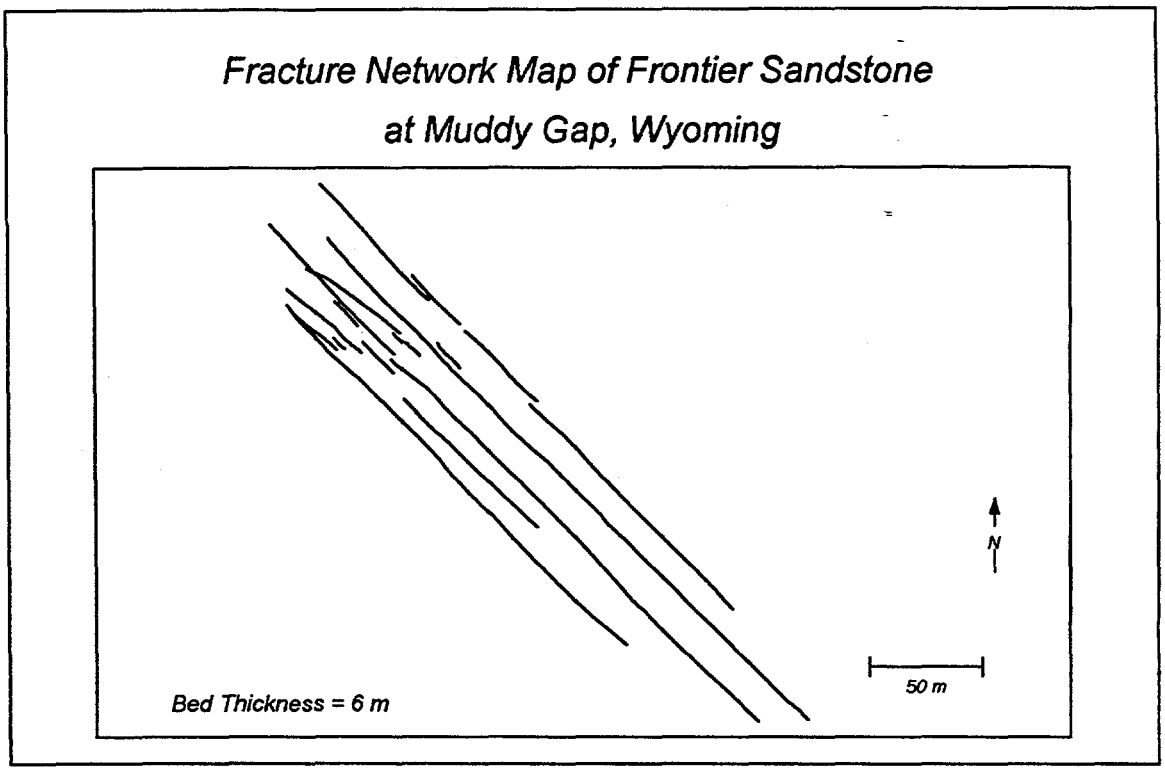

Figure 4.6. Fracture network map made of the outcrop at Muddy Gap, 110 km north of Rawlins on US Highway 287, Wyoming. The regional fracture network at this outcrop is a well-developed subparallel fracture set. Fracture length and spacing are the greatest of the outcrops studied. Fractures at this outcrop are also vertically continuous through the sandstone bed and terminate at the underlying shale. The azimuth of the regional fracture trend is N44°W. The estimated bed thickness is also the greatest of the four outcrops and is about 6 m.

4.3 Influence of Bed Thickness

The intensity of natural fractures will be influenced by several factors. Nelson (1985) listed the following parameters that can affect for fracture spacing:

1. Composition
2. Grain size
3. Porosity
4. Bed thickness
5. Structural position

Figure 4.8 shows the bed-thickness is a major controlling factor for fracture spacing, in this field-study of regional extension fractures.

Local variation in fracture intensity will give a fracture spacing dependent on where the scanline is laid, the scan line therefore has to be positioned to represent the average fractures or more than one line has to be drawn. The spacing presented in Figure 4.8

represents average spacing for each mapped outcrop section. For the bed thickness of 2 m the variation in spacing represents six mapped sections from the outcrop at Bridger Gap.

An important conclusion to this field study for the reservoir engineer is that regional fractures in Frontier sandstone reservoirs cannot be modeled with simple geometric models that are currently being used in dual-porosity reservoir simulations. Another approach must be taken if the bulk permeability of a naturally-fractured reservoir is to be calculated and fluid-flow response during reservoir production is to be realistically modeled. The next chapter will present an alternative approach to calculating fracture permeability using the tensor analysis method.

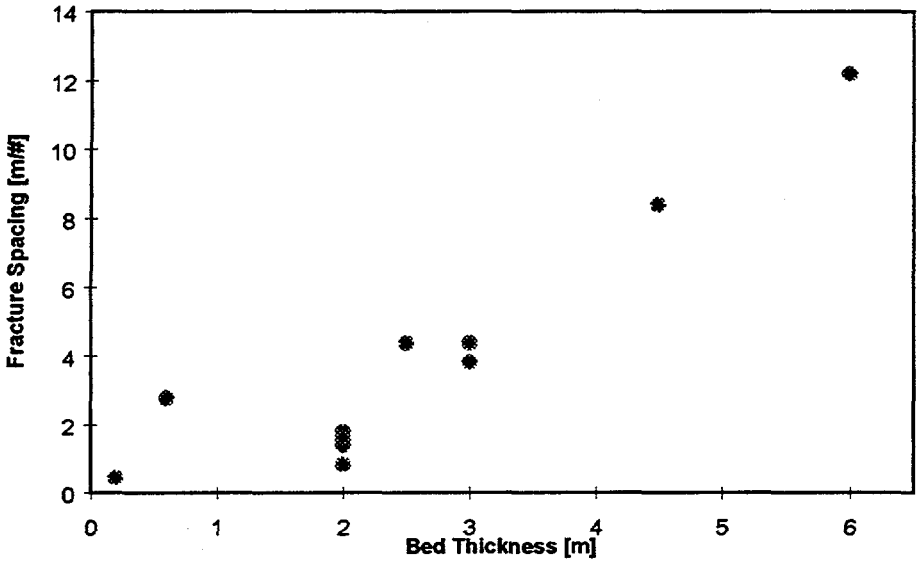

Figure 4.7. Fracture spacing increases with increasing bed thickness. Fracture spacing is average length in-between fractures measured along a scanline laid perpendicular to the regional fracture trend.

5. Permeability Calculations for Fractured Reservoirs

Calculating fluid flow in fractured reservoirs is difficult because of the complex spatial and geometrical properties of three-dimensional fracture networks. Creating a realistic fracture network model from outcrops or core data and incorporating this fracture network directly into a reservoir simulation model that honors the observed geologic data is an impossible task. Accordingly, reservoir engineers have traditionally approached reservoir simulation of fractured reservoirs by using a highly simplified, dual-porosity model based on the work of Muskat (1949). Parsons (1966) and others extended this work, and developed equations to describe fluid flow through fractures that are idealized as parallel plates. Reiss (1980) refined this approach and presented parallel-plate models for different, simple geometric configurations.

5.1 Dual-Porosity Models

The uniform permeability (in millidarcy) of individual fractured samples, k_s, assuming no matrix permeability, can be estimated from the following equation (Muskat, 1949):

$$k_s = \frac{54.52 * 10^9}{A} \sum_{i=1}^{N} L_i * w_i^3 \qquad (5.1)$$

A - domain area
N - number of fractures in unit
L_i - length of ith fracture
w_i - width of ith fracture
54.52×10^9 - convert from square inches to millidarcy

Equation (5.1) gives the fracture permeability assuming uniform permeability distribution in a continuous fracture network with an impermeable matrix. Reiss (1980), following the work of Parsons (1966) and others, set up the equations for fluid flow between parallel plates for the three basic cases (Figure 5.1).

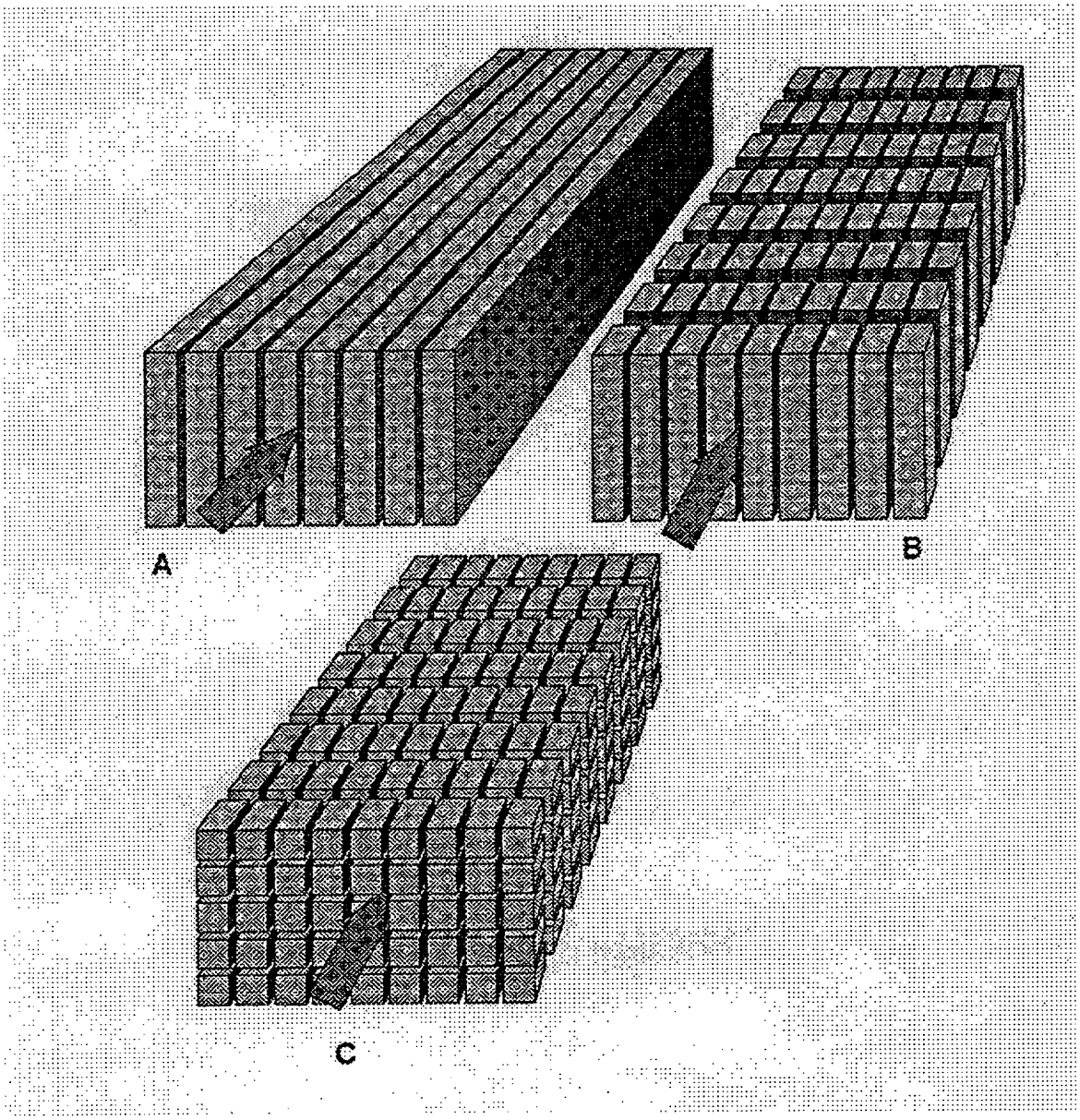

Figure 5.1. Three basic flow systems, A; Sheet, B; Match-sticks, C; Cubes.

(A). "Sheets" of matrix separated by parallel fracture planes, with fluid flow parallel to the fractures:

$$k_f = 8.33 * 10^3 a^2 \varnothing_f^{\,3}$$
$$\varnothing_f = \frac{b}{a} \qquad (5.2)$$

(B) "Match-sticks" separated by two orthogonal fracture planes:

$$k_f = 1.04 * 10^3 a^2 \varnothing_f^3$$
$$\varnothing_f = \frac{2b}{a} \qquad (5.3)$$

(C) "Cubes" separated by three orthogonal fractures

$$k_f = 0.62 * 10^{-12} a^2 \varnothing_f^3$$
$$\varnothing_f = \frac{3b}{a} \qquad (5.4)$$

k_f = permeability, md
$\varnothing_f$ = fracture porosity
a = dimension of uniform matrix block, cm
b = aperture, microns

This approach in calculating the permeability from a fracture network is a major simplification. It is valid only in cases in which the fracture network consists of regularly spaced, through-going fractures that are either parallel or orthogonal, with specific geometries, and constant aperture width.

Calculating fluid flow in fractured reservoirs is difficult because of the complex spatial and geometrical properties of three-dimensional fracture networks. Creating a realistic fracture network model from outcrops or core data and incorporating this fracture network directly into a reservoir simulation model that honors the observed geologic data is a difficult task (Figure 5.2).

An alternative approach is to replace a fractured medium by an unfractured porous medium which behaves equivalently (in sense of flow rate and pressure gradient) to the original fractured medium. This replacement is achieved by transforming the description of various fracture lengths, orientations, and apertures into an equivalent, anisotropic permeability tensor according to certain deterministic or stochastic procedures. In this study fracture characteristics from outcrops were coupled with Oda's (1985, 1986) algorithm to determine the magnitude and direction of the equivalent permeability. A brief description of the Muskat and Reiss fracture models will be presented, followed by the theory of Oda's permeability tensor method.

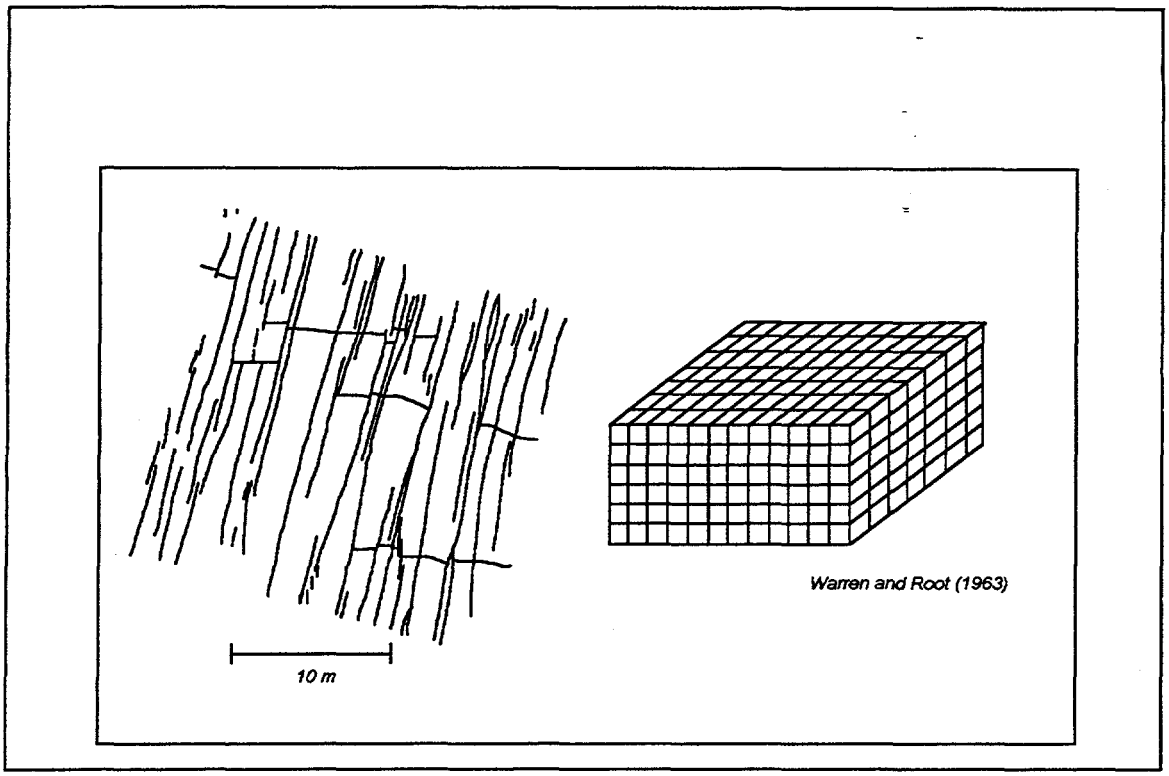

Figure 5.2. Applying fracture characterization to reservoir modeling. A conventional sugar-cube fracture model cannot account for the variation in fracture spacing. length, orientation and intensity as seen in the fracture outcrop maps.

5.2 Theory of Tensor Analysis

This section gives a summary of Oda's (1985, 1986) derivation of permeability tensors. Oda (1985, 1986) proposed a theory in which discontinuous rock masses are treated as homogeneous, anisotropic porous media. By using the tensor notation a representation of the permeability direction, magnitude and anisotropy can be given. If a fractured rock mass can be assumed to be a homogeneous, anisotropic porous medium, it obeys Darcy's law in which the apparent seepage velocity v_i vector is related to the gradient $-d\phi/dx_i$ of total hydraulic head ϕ, through a linking coefficient k_{ij} called the permeability tensor

$$\overline{v_i} = -\frac{g}{\nu} k_{ij} \frac{\partial \phi}{\partial x_i} = \frac{g}{\nu} k_{ij} J_i \qquad (5.5)$$

where g is the gravitational acceleration, ν is the kinematic viscosity and J_i is $-d\phi/dx_i$ (e.g. Scheidegger, 1957; Bear, 1972). Let us consider a flow domain having a representative elementary volume V. For fluid flow through cracks the apparent flow velocity is given by taking the average of the local velocity $v_i^{(c)}$ over the volume $V^{(c)}$ of the associated joints:

$$\bar{v}_i = \frac{1}{V}\int_V v_i dV$$
$$\bar{v}_i = \frac{1}{V}\int_{V^{(c)}} v_i^{(c)} dV^{(c)} \qquad (5.6)$$

Here, $v_i^{(c)}$ is the local velocity in the cracks and $V^{(c)}$ is the volume associated with the cracks. To use equation (5.6), attention is focused for the moment on (n,r,t) cracks characterized in the following manner. The unit vectors normal to the cracks are oriented inside a small solid angle $d\Omega$ around n, and the diameters and the apertures range from r to r + dr and from t to t + dt respectively. The aperture, t of a joint is difficult to define precisely because it is commonly unevenly undulated to make contact areas at various scales and is also partially filled by mineralization. Now, the probability density function E(n,r,t) is introduced in such a way that $2E(n,r,t)d\Omega drdt$ gives the probability of (n,r,t) cracks. It satisfies

$$\int_0^\infty\int_0^\infty\int_{\Omega/2} 2E(n,r,t)d\Omega drdt = \int_0^\infty\int_0^\infty\int_{\Omega} E(n,r,t)d\Omega drdt = 1 \qquad (5.7)$$

where $\Omega/2$ is the half of Ω corresponding to the surface of a hemisphere.

Let dN be the number of (n,r,t) cracks whose centers are located inside the flow region of volume V. To estimate the number, the probability of (n,r,t) cracks is multiplied by the total number of joints in the volume V, $m^{(V)}$.

$$dN = 2m^{(V)}E(n,r,t)d\Omega drdt \qquad (5.8)$$

Since each (n,r,t) crack produces a void volume equal to $(\pi/4)r^2t$ (for a penny shaped fracture), the total void volume $dV^{(c)}$ associated with the (n,r,t) cracks is given by

$$dV^{(c)} = \frac{\pi r^2 t}{4} dN = \frac{\pi m^{(V)}}{2} r^2 t E(n,r,t)d\Omega drdt \qquad (5.9)$$

Next consider the flow velocity suitable for (n,r,t) cracks. The flow region considered here consists of two constant head boundaries ($\phi_1 > \phi_2$) and four boundaries with the same linear variation in head from ϕ_1 to ϕ_2, so that the gradient J is given by

$$J = \frac{\phi_1 - \phi_2}{L} p \qquad (5.10)$$

where L is the distance between the two constant head boundaries and p is a unit vector pointing to J. The distribution of the head inside the flow region depends entirely on the hydraulic response of the crack system. Here it is assumed that the head linearly decreases, i.e. the field gradient J is uniform over the whole flow region. This assumption has been supported

by Long et al. (1982) on the basis of analysis of permeability in cracked media. Now let $J^{(c)}$ be a component of J projected on a (n,r,t) crack

$$J^{(c)} = J - (n * J)n \tag{5.11a}$$

or alternatively

$$J_i^{(c)} = (\delta_{ij} - n_i n_j)J_i \tag{5.11b}$$

where δ_{ij} is the Kronecker delta and n_i and J_i respectively are components of n and J projected on the orthogonal reference axis x_i (i = 1, 2, 3). The flow velocity for (n,r,t) cracks is given as

$$v_i^{(c)} = \lambda \frac{g}{\nu} t^2 J_i^{(c)} \tag{5.12}$$

where λ is a dimensionless constant with the restriction $0 < \lambda \leq 1/12$. Where 1/12 is the upper limit identical to laminar flow along a single fracture.

Substituting $J_i^{(c)}$ of equation (5.11) in equation (5.12), the apparent velocity associated with (n,r,t) cracks is finally written as

$$v_i^{(c)} = \lambda \frac{g}{\nu} t^2 (\delta_{ij} - n_i n_j)J_i \tag{5.13}$$

Using equations (5.9) and (5.13), equation (5.5) becomes

$$\bar{v}_i = \frac{1}{V}\int_{V^{(c)}} v_i^{(c)} dV^{(c)} = \lambda \frac{g}{\nu}\left[\frac{\pi\rho}{4}\int_0^{\infty}\int_0^{\infty}\int_{\Omega} r^2 t^3 (\delta_{ij} - n_i n_j) * E(n,r,t) d\Omega dr dt\right] J_i \tag{5.14}$$

where ρ is the volume density of cracks defined by

$$\rho = \frac{m^{(V)}}{V} \tag{5.15}$$

The integration is carried out over all cracks in the flow region.

A comparison between equation (5.14) and Darcy's law (equation (5.5)) leads to an equivalent permeability tensor $k_{ij}^{(c)}$ responsible for the crack system, as follows

$$k_{ij}^{(c)} = \lambda(P_{kk}\delta_{ij} - P_{ij}) \tag{5.16}$$

where

$$P_{ij} = \frac{\pi\rho}{4}\int\int\int r^2 t^3 n_i n_j E(n,r,t)\,d\Omega\,dr\,dt \tag{5.17}$$

The notation P_{ij}, which is tentatively called the 'crack tensor', is a symmetric, second rank tensor relating only to the crack geometry, i.e. to the crack shape, crack size, aperture and orientation. The number $\pi/4$ in equation (5.17) comes from the shape of cracks and is used for a penny shaped crack. To represent a square fracture $\pi/4$ is omitted.

Equation (5.16) is formulated on the basic assumption that the flow region is fully divided by cracks so that there are many flow paths within the region. The final equation produces a non-zero permeability even when P_{ij} becomes negligibly small. In reality, however, the flow region may become impermeable because the connectivity is completely lost in spite of the presence of cracks. To correct this shortcoming, the following modification is given: the crack tensor P_{ij} is decreased in such a way that it is multiplied by a positive scalar α that is less than unity. A threshold value can be observed at $\alpha = \alpha_0$ below which the region becomes practically impermeable because of the complete loss of the connectivity between cracks. Then, a correction term a_{ij} is introduced such that when $\alpha > \alpha_0$

$$k_{ij}^{(c)} = \lambda(P_{kk}\delta_{ij} - P_{ij}) + a_{ij} \tag{5.18a}$$

and when $0 < \alpha \leq \alpha_0$

$$k_{ij}^{(c)} = 0 \tag{5.18b}$$

Since $k_{ij}^{(c)} = 0$ at $\alpha = \alpha_0$, the correction term becomes

$$a_{ij} = -\lambda\alpha_0(P_{kk}\delta_{ij} - P_{ij}) \tag{5.19}$$

Substituting this in equation (5.21), the permeability tensor is finally given by

$$k_{ij}^{(c)} = \lambda(1-\alpha_0)(P_{kk}\delta_{ij} - P_{ij}) = \lambda(\overline{P}_{kk}\delta_{ij} - \overline{P}_{ij}) \tag{5.20}$$

where $\overline{P}_{ij} = P_{ij} - P_{ij}^{(0)}$, and $P_{ij}^{(0)} = \alpha_0 P_{ij}$. Here, $P^{(0)}$ gives a threshold, in the sense that the mass becomes impermeable if the corresponding crack tensor is less than $P_{ij}^{(0)}$. For the case where the flow region is fully divided by many large cracks, $P_{ij}^{(0)}$ can be set to zero because it becomes very small compared with P_{ij}, and therefore equation (5.16) with $\lambda = 1/12$ is used.

For a permeable matrix equation (5.6) the kinematic velocity is rewritten as a function of matrix and fracture flow velocity

$$\bar{v}_i = \frac{1}{V}\int_V v_i dV$$

$$\bar{v}_i = \frac{1}{V}\left(\int_{V^{(m)}} v_i^{(m)} dV^{(m)} + \int_{V^{(c)}} v_i^{(c)} dV^{(c)}\right) \tag{5.21}$$

where m denotes matrix and c crack or fracture. Equation (5.21) corresponds to an assumption that the non-steady interaction between the double porosities can be neglected. Since the permeable matrix behaves like an ideal porous medium, there must be a complementary permeability tensor $k_{ij}^{(m)}$. The void volume $V^{(c)}$ associated with the cracks is usually so small that $V^{(m)}$ is nearly equal to V. Then, equation (5.21) becomes

$$\bar{v}_i = \frac{1}{V}\left(\int_V v_i^{(m)} dV^{(m)} + \int_{V^{(c)}} v_i^{(c)} dV^{(c)}\right)$$

$$\bar{v}_i = \frac{g}{\nu}\left(k_{ij}^{(m)} + k_{ij}^{(c)}\right)J_i \tag{5.22}$$

Now substituting P_{ij}, together with λ and t in

$$k_{ij}^{(c)} = \lambda(P_{kk}\delta_{ij} - P_{ij}) \tag{5.16}$$

which gives

$$k_{ij} = \begin{bmatrix} k_{11} & k_{12} \\ k_{21} & k_{22} \end{bmatrix} \tag{5.23}$$

$$k_x = \frac{1}{2}(k_{11} + k_{22}) + \sqrt{k_{12}^2 + \frac{1}{4}(k_{11} - k_{22})^2}$$

$$k_y = \frac{1}{2}(k_{11} + k_{22}) - \sqrt{k_{12}^2 + \frac{1}{4}(k_{11} - k_{22})^2} \tag{5.24}$$

$$k_{ij} = \begin{bmatrix} k_x & 0 \\ 0 & k_y \end{bmatrix} \tag{5.25}$$

Where k_x and k_y represent the two dimensional, directional permeability.

5.3 Assumptions

To perform the derivation certain assumptions have to be made. At the outcrops the fracture networks are studied at surfaces parallel to bedding, which gives a two-dimensional entities, which imposes additional assumptions and are noted by (2-D).

1. Non-steady interaction between the double porosities can be neglected.
2. Each crack can be replaced by parallel planar plates.
3. No head loss at intersections between joints.
4. Fractures extend the full thickness of the reservoir bed, vertical continuity (2-D).
5. Constant fracture aperture (2-D) along individual fractures and for each fracture.

5.4 Applying Oda's Model to Field Data

To analyze the field data the "Two Dimensional Fracture Network Analysis" program for Oda's model, developed by R. Bruhn (University of Utah), is applied. The calculation steps are given below for the fracture network at Flaming Gorge.

1. Read the fracture data file (Table 5.1), measured fracture orientation (θ) and measured length (L), enter assumed constant aperture width ($t_0 = 0.1$ mm) and the measured area of the plan view rock face ($A = 929$ m^2). Enter the matrix permeability ($k_m = 1\times10^{-17}$ m^2) which will be added to fracture permeability. Since the sandstone studied is interbedded with shale and the fracture length is an order of magnitude greater than the bed thickness, the fracture geometry can be represented by length and orientation as measured at the bed surface, height equal to bed thickness, and by constant aperture ($t = t_0$).

2. Compute the fracture volume and porosity

$$V^{(f)} = \sum_{k=1}^{N} t \times L_k = \sum_{k=1}^{N} 0.0001 \times L_k = 0.0001 \times 267.94 = 0.026794 \qquad (5.26)$$

$$\varnothing^{(f)} = \frac{V^{(f)}}{A} \times 100\% = \frac{0.026794}{929} \times 100 = 0.002884\% \qquad (5.27)$$

3. Angles are converted into radians and the direction cosines of the fracture pole to the fracture trace is computed (Table 5.2). For an angle of 40^0:

$$\omega = \theta\frac{\pi}{180} = 40^0\,\frac{3.1415}{180} = 0.6981$$
$$n_i = -\sin(\omega) = -\sin(0.6981) = -0.6428$$
$$n_j = \cos(\omega) = \cos(0.6981) = 0.7660$$

4. Compute the four components of the two dimensional fabric tensor F_{ij}, related to the crack geometry:

$$F_{ij} = \frac{\sum_{k=1}^{N} L_k^2 n_i n_j}{A} \qquad (5.28)$$

$$F_{ij} = \begin{bmatrix} F_{11} & F_{12} \\ F_{21} & F_{22} \end{bmatrix} = \begin{bmatrix} 2.1114 & -2.6902 \\ -2.6902 & 3.4530 \end{bmatrix} \tag{5.29}$$

5. Find the principle values F_1 and F_2 of the fabric tensor, F_{ij}:

$$F_1 = \frac{1}{2}(F_{11} + F_{22}) + \sqrt{F_{12}{}^2 + \frac{1}{4}(F_{11} - F_{22})^2}$$

$$F_1 = \frac{1}{2}(2.1114 + 3.4530) + \sqrt{-2.6902^2 + \frac{1}{4}(2.1114 - 3.4530)^2}$$

$$F_1 = 5.5547 \tag{5.30}$$

$$F_2 = \frac{1}{2}(F_{11} + F_{22}) - \sqrt{F_{12}{}^2 + \frac{1}{4}(F_{11} - F_{22})^2}$$

$$F_2 = \frac{1}{2}(2.1114 + 3.4530) - \sqrt{-2.6902^2 + \frac{1}{4}(2.1114 - 3.4530)^2}$$

$$F_2 = 0.0096$$

$$F_{ij} = \begin{bmatrix} F_1 & 0 \\ 0 & F_2 \end{bmatrix} = \begin{bmatrix} 5.5547 & 0 \\ 0 & 0.0096 \end{bmatrix} \tag{5.31}$$

6. Compute the first invariant of the fabric tensor, F_0 and the anisotropy index $A^{(F)}$:

$$F_0 = F_1 + F_2 = 5.5547 + 0.0096 = 5.5643 \tag{5.32}$$

$$A^{(F)} = \frac{F_1 - F_2}{F_1 + F_2} = \frac{5.5547 - 0.0096}{5.5547 + 0.0096} = 0.9965 \tag{5.33}$$

($A^{(F)} = 1$ for isotropic fracture system, $1 > A^{(F)} > 0$ for anisotropic fracture system).

7. Convert direction cosines in x-y plane into angle in degrees.

8. Compute the four components of the two dimensional P-tensor (Figure 5.3):

$$P_{ij} = \frac{\sum_{k=1}^{N} t^3 L_k \times n_i n_j}{A} = \frac{0.0001^3}{929} \sum_{k=1}^{N} L_k \times n_i n_j \tag{5.34}$$

$$P_{ij} = \begin{bmatrix} P_{11} & P_{12} \\ P_{21} & P_{22} \end{bmatrix} = \begin{bmatrix} 0.1120 \times 10^{-12} & -0.1398 \times 10^{-12} \\ -0.1398 \times 10^{-12} & 0.1764 \times 10^{-12} \end{bmatrix}$$

9. Find the value of lambda based on regression of lambda vs. F_0 (Oda et al., 1987):

$$\begin{aligned} \lambda &= 0.0210 + 0.0017 * F_0 \\ \lambda &= 0.0210 + 0.0017 \times 5.5643 \\ \lambda &= 0.03046 \end{aligned} \tag{5.35}$$

10. Compute the bulk permeability tensor which includes the matrix permeability added to the fracture permeability tensor:

$$k_{ij}^{(f+m)} = \lambda(\overline{P}_{kk}\delta_{ij} - \overline{P}_{ij}) + k^{(m)} * \delta_{ij} \tag{5.36}$$

$$k_{ij}^{(f+m)} = 0.03046 \times 10^{-12}\left(\left[0.1120 + 0.1764\right] \times \delta_{ij} - \begin{bmatrix} 0.1120 & -0.1398 \\ -0.1398 & 0.1764 \end{bmatrix}\right) + 10^{-17} \times \delta_{ij}$$

$$k_{ij}^{(f+m)} = \begin{bmatrix} k_{11} & k_{12} \\ k_{21} & k_{22} \end{bmatrix} = \begin{bmatrix} 5.383 & 4.257 \\ 4.257 & 3.422 \end{bmatrix} \times 10^{-15}$$

11. Compute the directional permeability and select the reference axes as the principal axes x_1' and x_2' of the crack tensor:

$$\beta = \frac{1}{2}\arctan\left(\frac{2k_{21}}{k_{11} - k_{22}}\right) = \frac{1}{2}\arctan\left(\frac{2 \times 4.257}{5.383 - 3.422}\right) = 38.51^0 \tag{5.37}$$

$$k_x = \frac{1}{2}\left(k_{11} + k_{22}\right) + \sqrt{k_{12}{}^2 + \frac{1}{4}\left(k_{11} - k_{22}\right)^2}$$

$$k_1 = \left(\frac{1}{2}(5.383 + 3.422) + \sqrt{4.257^2 + \frac{1}{4}(5.383 - 3.422)^2}\right) \times 10^{-15} \tag{5.24}$$

$$k_x = 8.771 \times 10^{-15}$$

$$k_y = \frac{1}{2}\left(k_{11} + k_{22}\right) - \sqrt{k_{12}{}^2 + \frac{1}{4}\left(k_{11} - k_{22}\right)^2}$$

$$k_y = \left(\frac{1}{2}(5.383 + 3.422) - \sqrt{4.257^2 + \frac{1}{4}(5.383 - 3.422)^2}\right) \times 10^{-15}$$

$$k_y = 0.034 \times 10^{-15}$$

$$k_{ij}^{(f+m)} = \begin{bmatrix} k_x & 0 \\ 0 & k_y \end{bmatrix} = \begin{bmatrix} 8.771 & 0 \\ 0 & 0.034 \end{bmatrix} \times 10^{-15}$$

The permeability tensor (k_x, k_y) is given with an angle β, rotated from the previous reference system.

Table 5.1 Fracture characterization from Flaming Gorge.

Fracture orientation (θ), relative to North	Measured length (L), meters
35	1.225406
62	1.494862
40	2.38515
39	3.496306
47	4.832662
40	5.769004
40	7.488262
40	7.821272
40	7.876739
40	7.988259
39.5	9.485297
40.5	10.76149
41	13.75667
39	15.31096
38	16.92539
34	17.59764
37	24.21271
39	24.79547
38	25.05524
34	27.21138
40	32.44956

Table 5.2 Direction cosines calculated from fracture characterization at Flaming Gorge

Angle (θ) [deg]	Angle (ω) [rad]	n_i	n_j
35	0.6109	-0.5736	0.8192
62	1.0821	-0.8829	0.4695
40	0.6981	-0.6428	0.766
39	0.6807	-0.6293	0.7771
47	0.8203	-0.7314	0.682
40	0.6981	-0.6428	0.766
40	0.6981	-0.6428	0.766
40	0.6981	-0.6428	0.766
40	0.6981	-0.6428	0.766

40	0.6981	-0.6428	0.766
39.5	0.6894	-0.6361	0.7716
40.5	0.7069	-0.6494	0.7604
41	0.7156	-0.6561	0.7547
39	0.6807	-0.6293	0.7771
38	0.6632	-0.6157	0.788
34	0.5934	-0.5592	0.829
37	0.6458	-0.6018	0.7986
39	0.6807	-0.6293	0.7771
38	0.6632	-0.6157	0.788
34	0.5934	-0.5592	0.829
40	0.6981	-0.6428	0.766

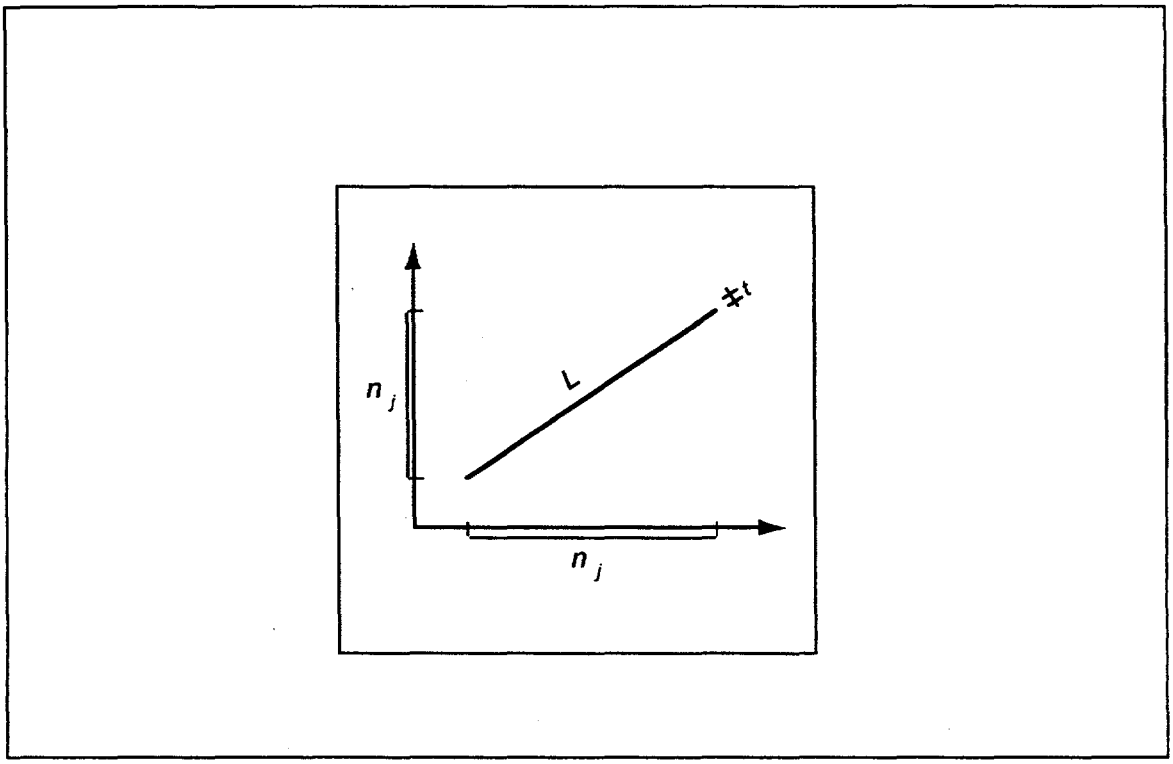

Figure 5.3 Fracture tensor. The two dimnensional fracture tensor is calculated based on fracture length, orientation and aperture width.

5.5 Comparison of Oda's Fracture Tensor Model with Dual-Porosity Model

Results of the permeability tensor method presented by Oda, was compared to a dual porosity model using Reiss's (1980) parallel-plate equations (section 5.1). The fracture network geometries for the two cases are shown in Figure 5.4 and consist of:

1. One set of fifty evenly spaced, vertical fractures.

2. Two orthogonal sets (50x50) of vertical fractures, which gives 2500 matrix blocks.
The simulation area is 10 m x 10 m. In both cases the fracture aperture is 0.1 mm (100 μm), modeling the fracture permeability, and the matrix is impermeable.

Figure 5.5 shows the fabric and permeability tensor for case 1, which is one set of fifty evenly spaced fractures. Permeability varies from a maximum of 4.165^{-13} m^2 (416.5 md) in the direction parallel to the fractures, to zero perpendicular to the fractures, and a fracture porosity of 0.05 % is used. This case is represented by Reiss (1980) as "sheets" of matrix separated by fracture planes with fluid flow parallel to the fractures. Using equations (5.2) the fracture permeability and porosity are:

$$k_f = 8.33 * 10^{-3} 20^2 0.05^3 = 416.5md$$

$$\varnothing_f = \frac{1}{100} \frac{50 * 100\mu m}{1000cm} = 0.05\%$$

which is the same as Oda's model.

Figure 5.6 shows the fabric and permeability tensor plots for the second case of two sets of fifty by fifty evenly spaced fractures. The results from the Oda model show a radial permeability distribution, as was expected, of 4.165×10^{-13} m^2 (416.5 md) with a 0.1 % porosity. This case is represented by Reiss's "match stick" model of two sets of orthogonal fracture planes. Using equation (5.3) the fracture permeability and fracture porosity are

$$k_f = 1.04 * 10^{-3} 20^2 0.1^3 = 416md$$

$$\varnothing_f = \frac{1}{100} \frac{2 * 50 * 100\mu m}{1000cm} = 0.1\%$$

which is also identical to Oda's model result. The results are summarized in table 5.3.

Table 5.3 Permeability calculations. For the sheet model there is no permeability perpendicular to the fracture trend.

	Case 1 Sheet model 50 fractures		Case 2 Match stick model 50×50 fractures	
Model	Reiss	Oda	Reiss	Oda
Fracture permeability [md]	416.5	416.5	416.5	416.5
Fracture porosity [%]	0.05	0.05	0.1	0.1

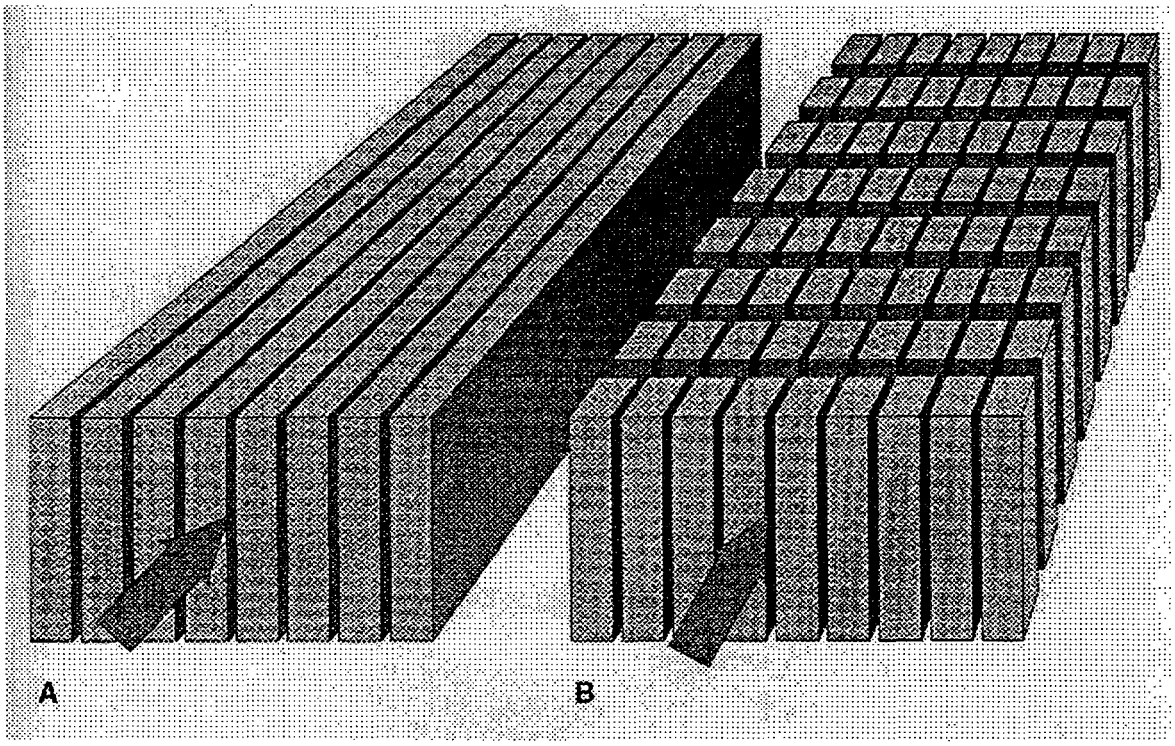

Figure 5.4. The two flow models, sheets (A) and match-sticks (B).

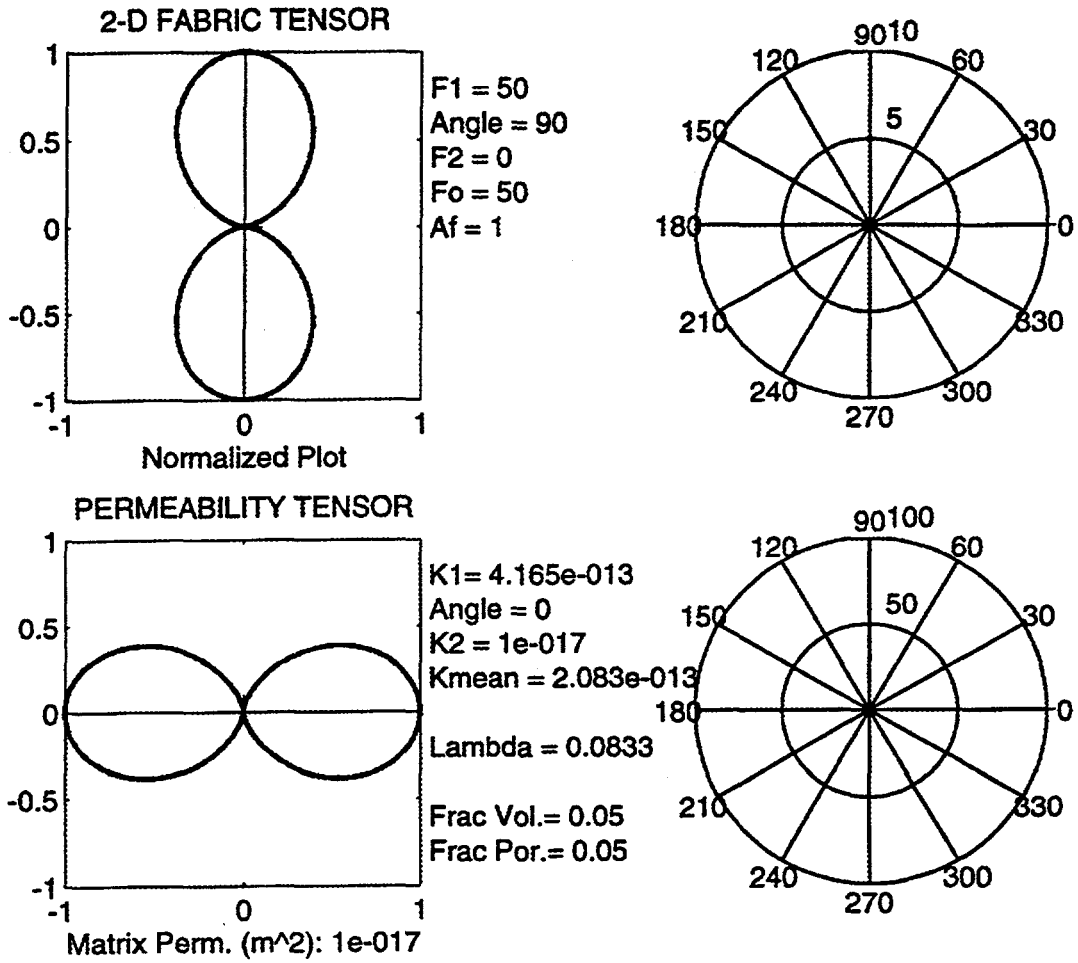

Figure 5.5. Plots of fabric tensor and permeability tensor for case 1; one set of fifty evenly spaced fractures. F_1 and F_2, are the eigenvectors of the fabric tensor, F_0 the first invariant of the fabric tensor, $A^{(F)}$ the anisotropy index, K_1 maximum permeability, K_2 minimum permeability, K_m average arithmetic permeability.

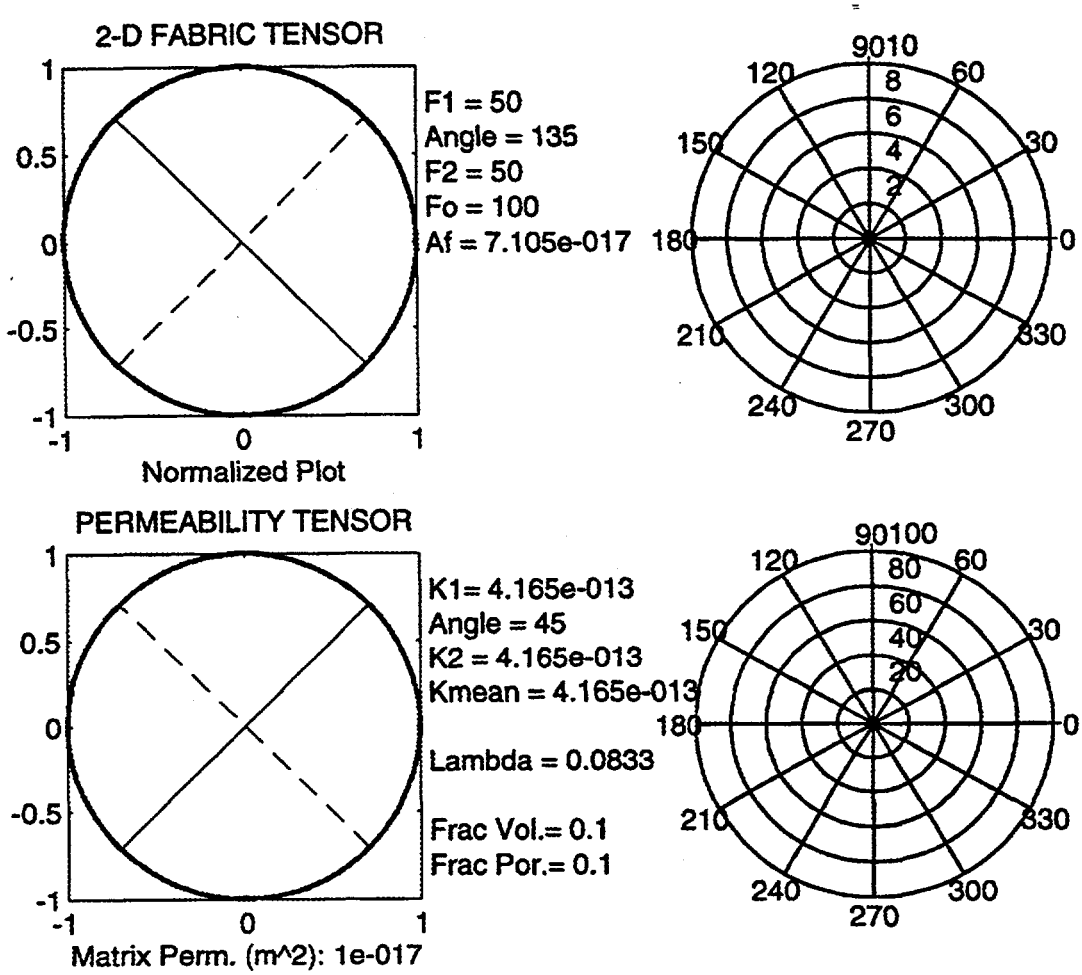

Figure 5.6. Plots of fabric tensor and permeability tensor for case 2; two sets of fifty by fifty evenly spaced fractures. F_1 and F_2, are the eigenvectors of the fabric tensor, F_0 the first invariant of the fabric tensor, $A^{(F)}$ the anisotropy index, K_1 maximum permeability, K_2 minimum permeability, K_m average arithmetic permeability.

6. Application of the Permeability Tensor Analysis

In this chapter fracture data for the regional fracture set obtained from the four outcrop fracture-network maps are combined with matrix permeability data to compute an anisotropic permeability tensor (magnitude and direction). This tensor corresponds to an analogous Frontier sandstone fracture system in the subsurface using Oda's permeability tensor method and Bruhn's computer program. The four cases have different bed thicknesses and a corresponding difference in fracture spacing and length. In each case the fractures are vertically continuous through the sandstone bed and terminate at the bounding shale layer. Fracture height is equal to bed thickness and is at least an order of magnitude less than fracture length. For this study the fracture aperture is assumed to be constant and equal to 0.1 mm, which is consistent with an average fracture aperture for natural fractures of sandstone reservoirs (Nelson, 1985). Matrix permeability is assumed to be isotropic and equal to 10^{-17} m^2 (10 μd), which is a typical matrix permeability of tight gas sandstones. Matrix porosity is estimated to be 14 %, which is a typical value for Frontier sandstones in the Green River Basin.

6.1 Results of Permeability Calculations

Figures 6.1 to 6.4 are plots of the fabric tensor and permeability tensor calculated for an equivalent reservoir volume corresponding to the regional fracture network area and bed thickness at each of the four outcrops. Table 6.1 summarizes the calculated results of the analysis for each outcrop fracture network and bed thickness.

For the regional fracture network at Scullys Gap (fracture network map is shown in Figure 4.3) the maximum horizontal permeability, k_x, is 154.3×10^{-15} m^2 with an azimuth of N19°E, which is, as expected, parallel to the regional fracture trend. Minimum horizontal permeability is 0.286×10^{-15} m^2 and is more than an order of magnitude greater than the matrix permeability. The horizontal permeability anisotropy is very large with the ratio of maximum to minimum permeability being 545 ($k_x/k_y = 545$).

For the regional fracture network at Bridger Gap (fracture network map is shown in Figure 4.4) the maximum horizontal permeability, k_x, is 33.63×10^{-15} m^2 with an azimuth of N12°E, which is also, as expected, parallel to the regional fracture trend. Minimum horizontal permeability is 0.062×10^{-15} m^2, which is six times greater than the matrix permeability. The horizontal permeability anisotropy is very large with the ratio of maximum to minimum permeability being 542.

For the regional fracture network east of Flaming Gorge (fracture network map is shown in Figure 4.5) the maximum horizontal permeability, k_x, is 8.771×10^{-15} m^2 with an azimuth of N38°W and is parallel to the regional fracture trend at this location. Minimum horizontal permeability is 0.034×10^{-15} m^2 and is only three times greater than the matrix permeability. The horizontal permeability anisotropy is less than the previous two cases with the ratio of maximum to minimum permeability being 258.

For the regional fracture network at Muddy Gap (fracture network map is shown in Figure 4.6) the maximum horizontal permeability, k_x, is 3.066×10^{-15} m^2 with an azimuth of N43°W and is parallel to the regional fracture trend at this location. Minimum horizontal permeability is 0.010×10^{-15} m^2 and is equal to the matrix permeability. The horizontal permeability anisotropy, the ratio of maximum to minimum permeability, is 307.

Table 6.1. Summary of calculated model results for fracture networks and bed thickness measured at five outcrops of the Frontier sandstone. Geometric mean permeability is used to calculate k in the flow capacity.

	Scullys Gap	Bridger Gap	Flaming Gorge	Salt Wells Creek	Muddy Gap
Bed Thickness, m (ft)	0.2 (0.66)	2 (6.6)	3 (10)	4.5 (15)	6 (20)
Area studied, m^2	78	929	929	1102	18755
k_x, 10^{-15} m^2	154.3	33.63	8.771	3.34	3.066
k_y, 10^{-15} m^2	0.286	0.062	0.034	0.0263	0.010
Permeability ratio, k_x/k_y	539.5	542.4	258.0	127.0	306.6
Direction of k_x	N19°E	N13°E	N39°W	N52°W	N44°W
k_{mean} (geometric), 10^{-15} m^2	6.64	1.44	0.55	0.30	0.18
Flow capacity (kh), md ft	4.38	9.5	5.5	4.5	3.6
Fracture Porosity, %	0.0234	0.0075	0.0029	0.0012	0.0007
Storage capacity (ϕh), m	0.028	0.28	0.42	0.63	0.84

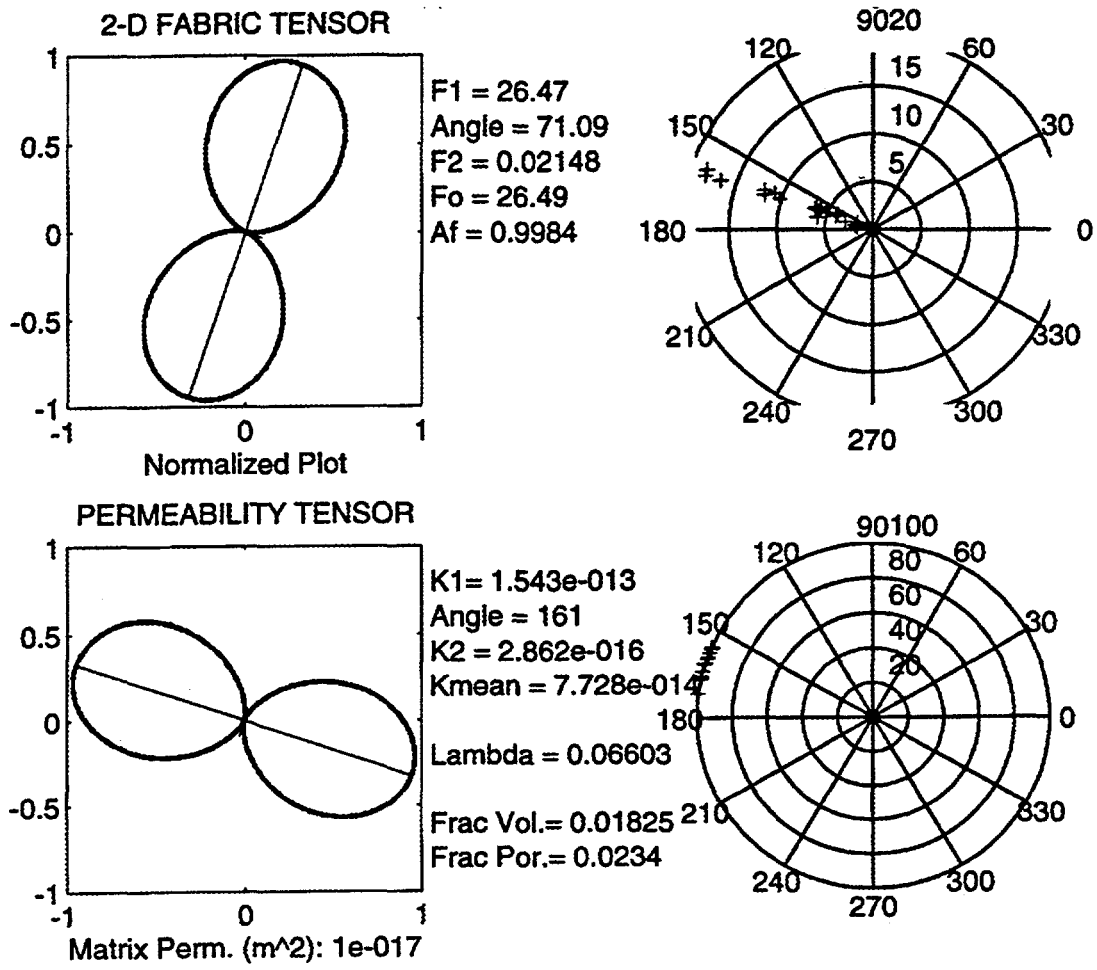

Figure 6.1. Plot of fabric tensor and permeability tensor for fracture network at Scullys Gap. F_1 and F_2, are the eigenvectors of the fabric tensor, F_0 the first invariant of the fabric tensor, $A^{(F)}$ the anisotropy index, K_1 maximum permeability, K_2 minimum permeability, K_m average arithmetic permeability.

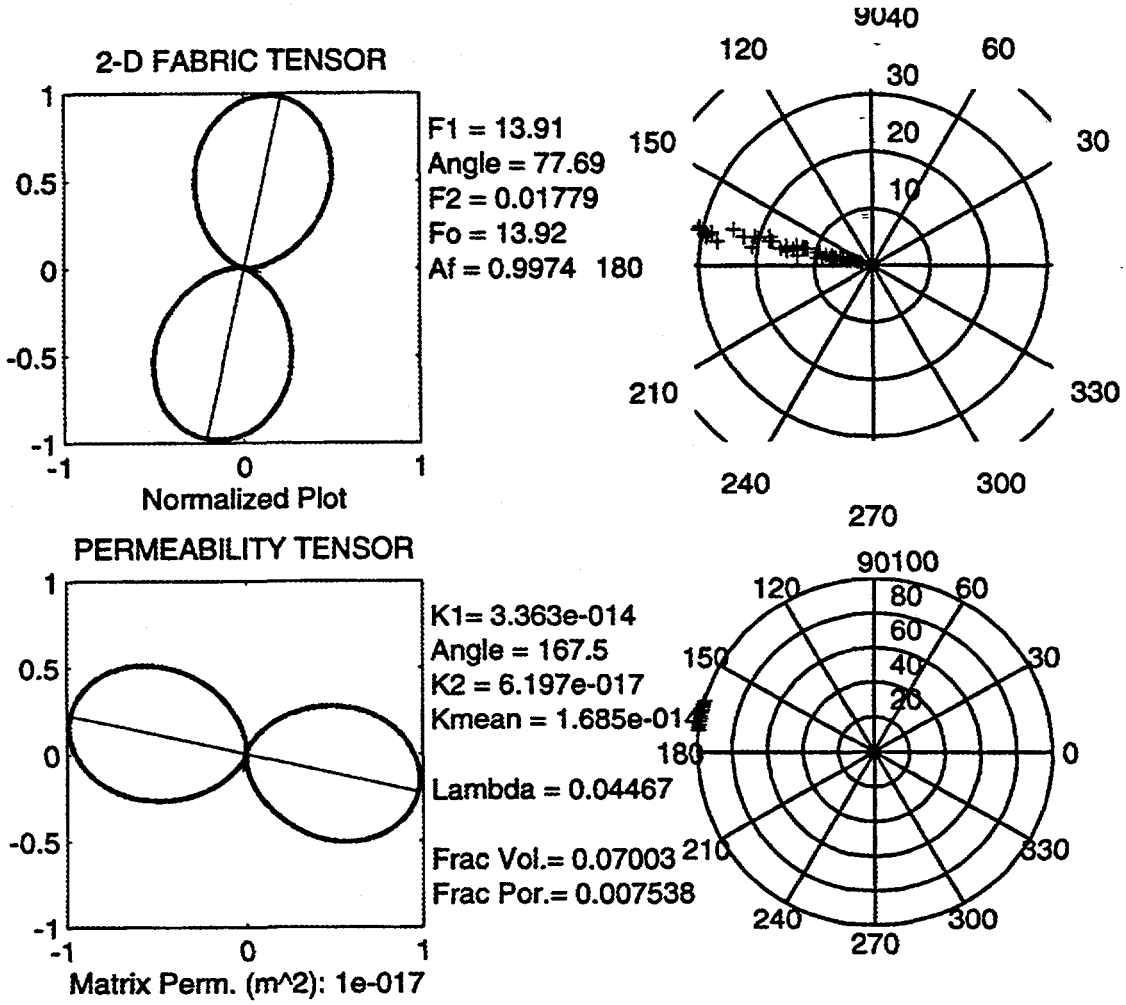

Figure 6.2. Plot of fabric tensor and permeability tensor for fracture network at Bridger Gap. F_1 and F_2, are the eigenvectors of the fabric tensor, F_0 the first invariant of the fabric tensor, $A^{(F)}$ the anisotropy index, K_1 maximum permeability, K_2 minimum permeability, K_m average arithmetic permeability.

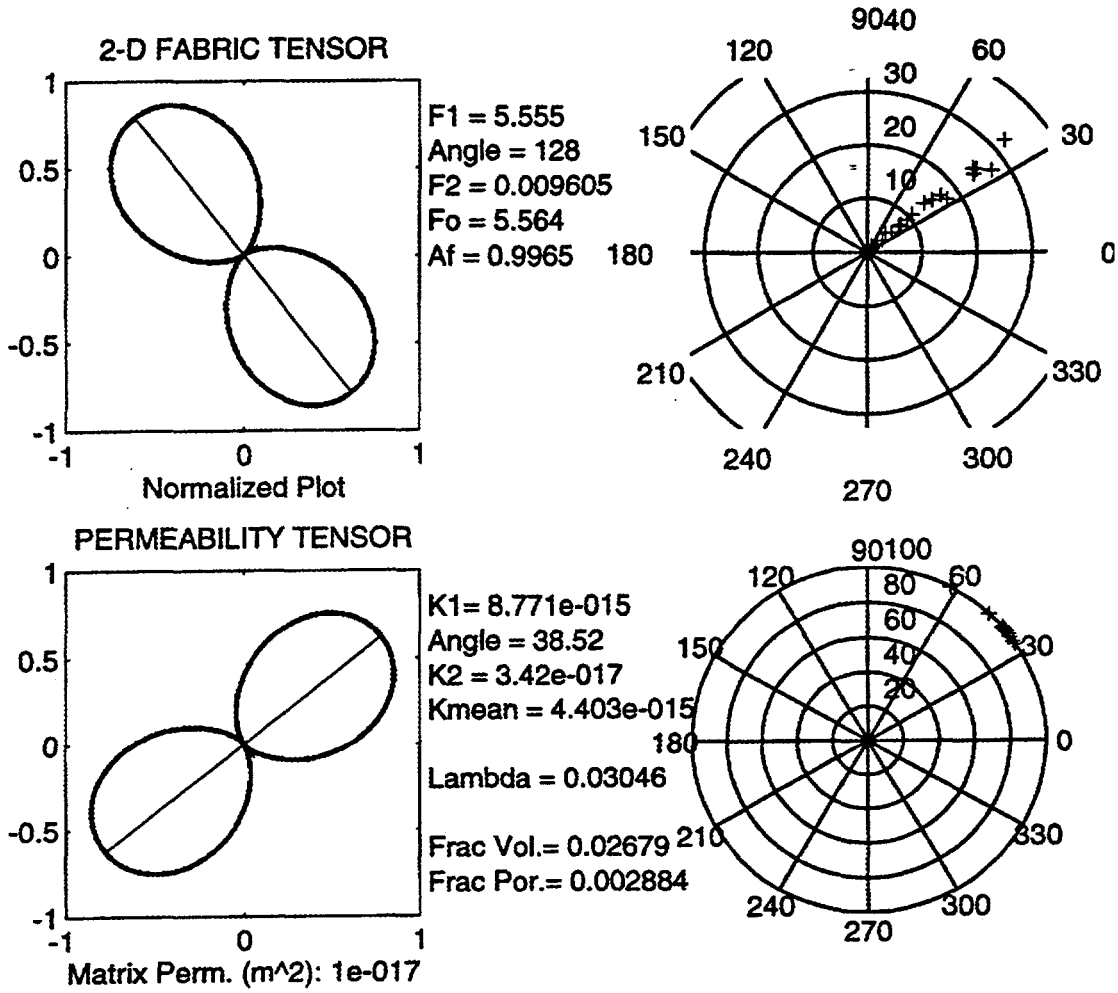

Figure 6.3. Plot of fabric tensor and permeability tensor for fracture network at east of Flaming Gorge. F_1 and F_2, are the eigenvectors of the fabric tensor, F_0 the first invariant of the fabric tensor, $A^{(F)}$ the anisotropy index, K_1 maximum permeability, K_2 minimum permeability, K_m average arithmetic permeability.

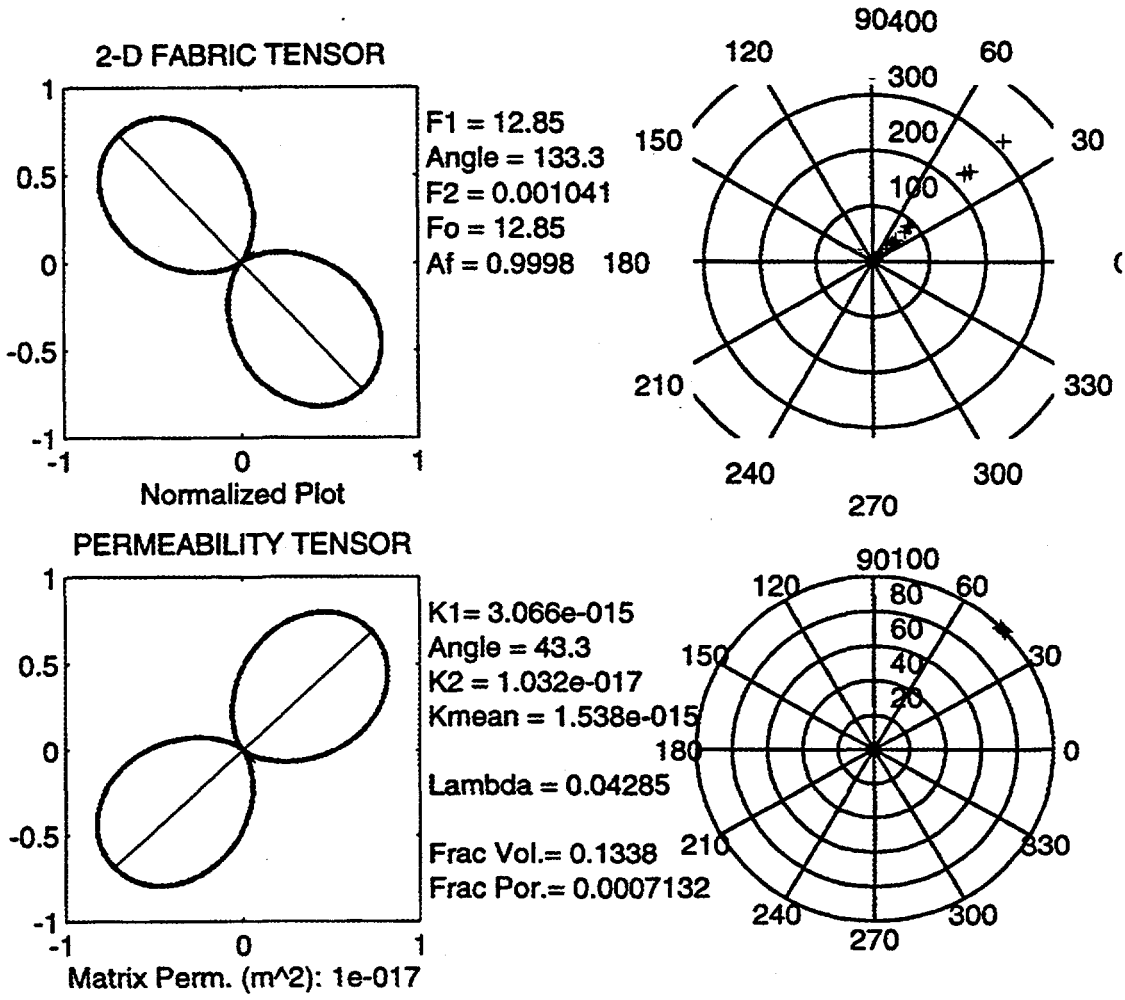

Figure 6.4. Plot of fabric tensor and permeability tensor for fracture network at Muddy Gap. F_1 and F_2, are the eigenvectors of the fabric tensor, F_0 the first invariant of the fabric tensor, $A^{(F)}$ the anisotropy index, K_1 maximum permeability, K_2 minimum permeability, K_m average arithmetic permeability.

6.2 Influence of Bed Thickness on Calculated Horizontal Permeability

The fracture network maps clearly show that fracture spacing and length are related to bed thickness. In general, fewer fractures occur per unit area as the bedding thickness increases. Moreover fractures do not have a consistent and equal spacing for a given bed thickness. The length of regional fractures is highly variable, but tends to increase with increasing bed thickness. The net result is that there are fewer and longer fractures per reservoir area and volume as the bed thickness increases. This change in the spatial distribution of fractures directly affects the calculated bulk permeability tensor and flow capacity of an equivalent reservoir volume in the subsurface.

Figure 6.5 shows the relationship between bed thickness and the calculated maximum horizontal permeability for reservoirs that are analogous to the outcrop fracture-networks. The maximum permeability decreases with increasing bed thickness from 154.3 md for a bed thickness of 0.2 m to 3.066 md for a bed thickness of about 6 m. Plotting bed thickness versus log of the maximum horizontal permeability gives a linear trend, indicating a logarithmic relationship (Figure 6.6). The rapid decline in maximum horizontal permeability is directly related to the decrease in fracture density with increasing bed thickness.

Minimum horizontal permeability also decreases with increasing bed thickness from 0.286 md to 0.010 md (matrix permeability) for the same change in bed thickness (Figure 6.7). The direction of the calculated minimum horizontal permeability is perpendicular to the regional fracture trend. The minimum horizontal permeability rapidly declines to the matrix permeability as the fracture spacing decreases with increasing bed thickness.

The calculated flow capacity for an equivalent reservoir volume is a function of the fracture intensity, and changes with bed thickness (Figure 6.8). Together with storage-capacity flow capacity defines the fluid flow response for a reservoir. In the next chapter we will use these two parameters to explain results from reservoir simulation.

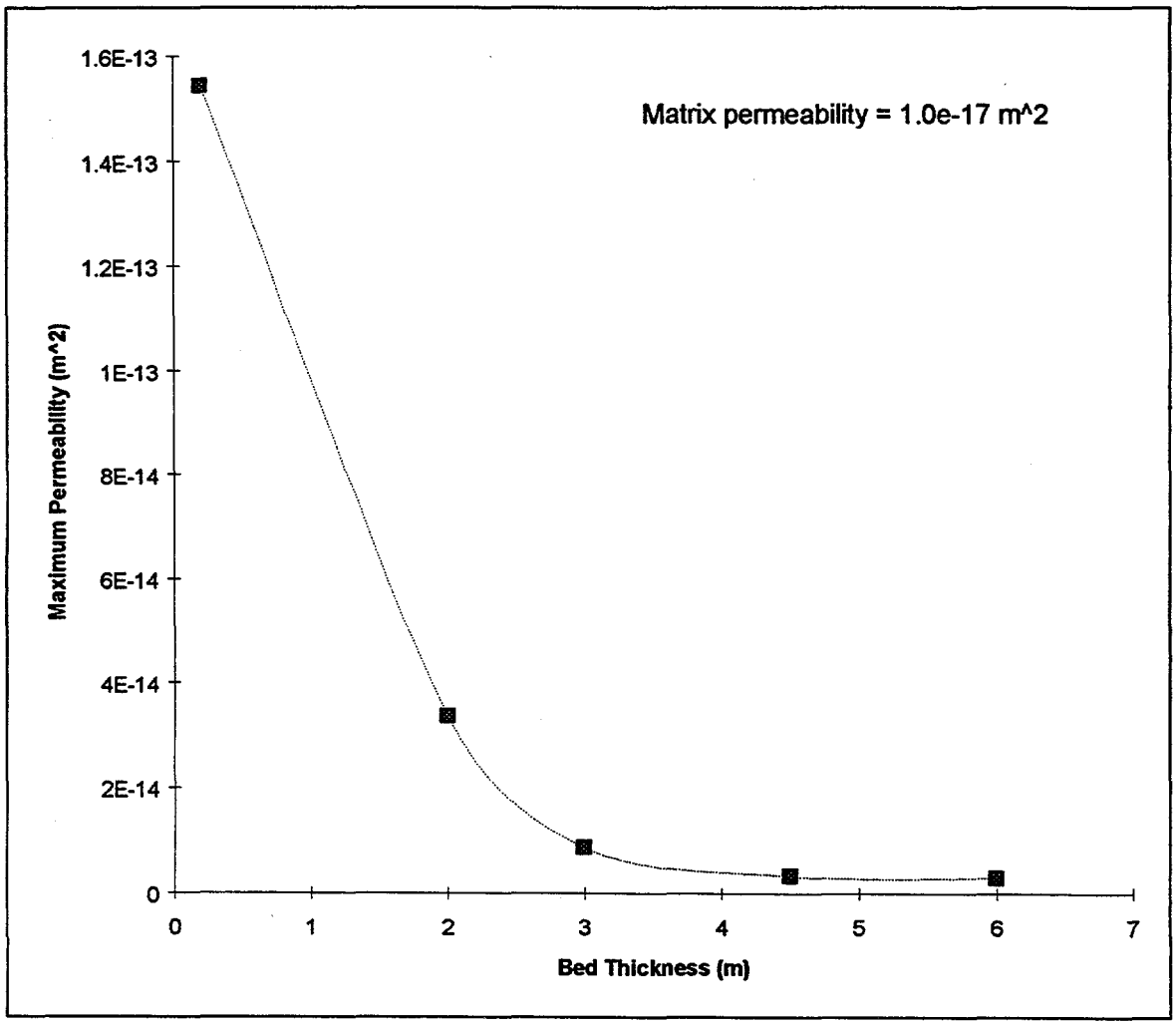

Figure 6.5. Plot of bed thickness versus calculated maximum horizontal permeability, k_x. There is a more than one order of magnitude drop in k_x from the thinnest bed of 0.2 m to the thickest of 6 m.

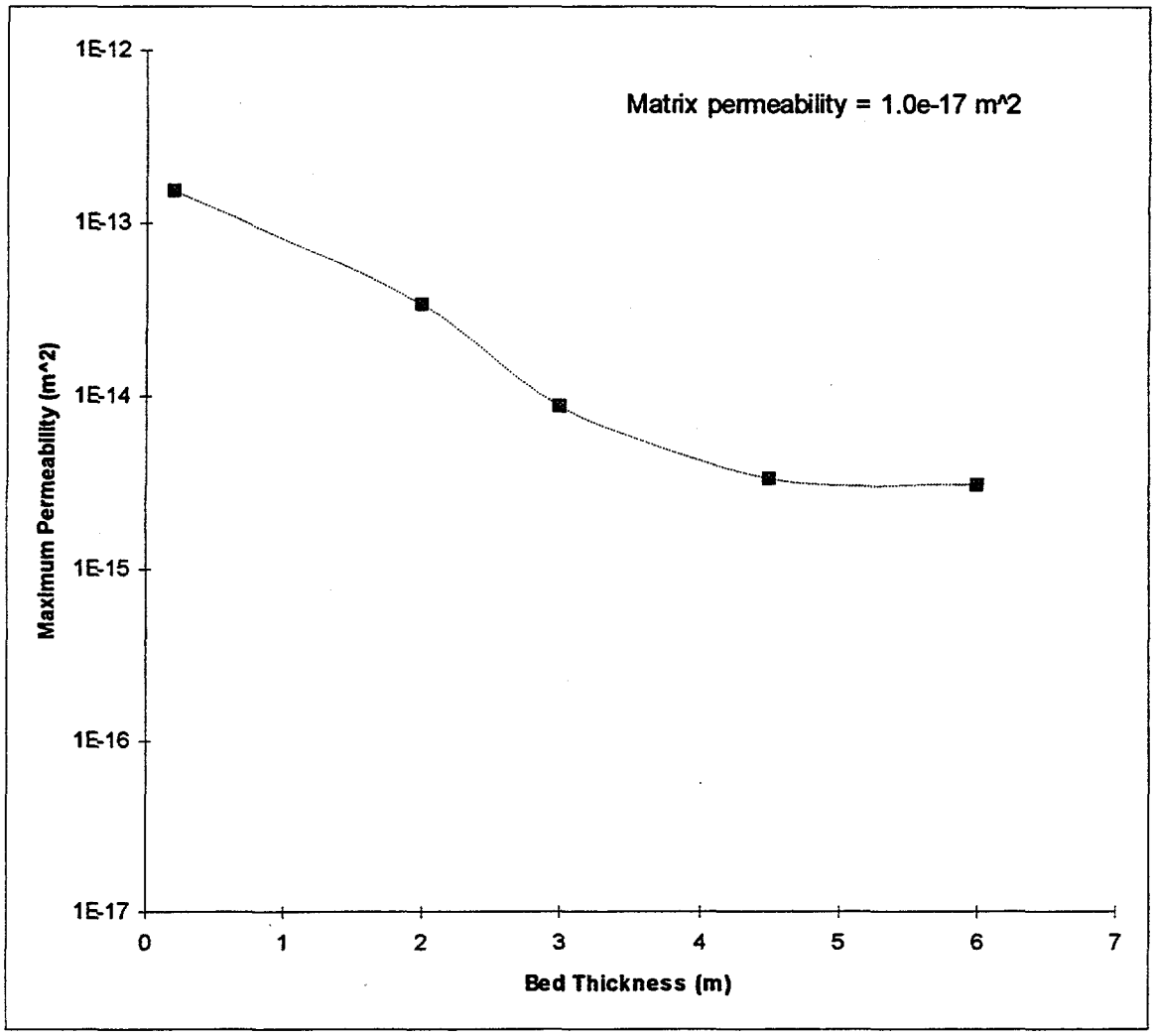

Figure 6.6. Bed thickness versus logarithmic maximum horizontal permeability, k_x. Note that for the bed thickness of 6 m, k_x is still two orders of magnitude higher than the matrix permeability.

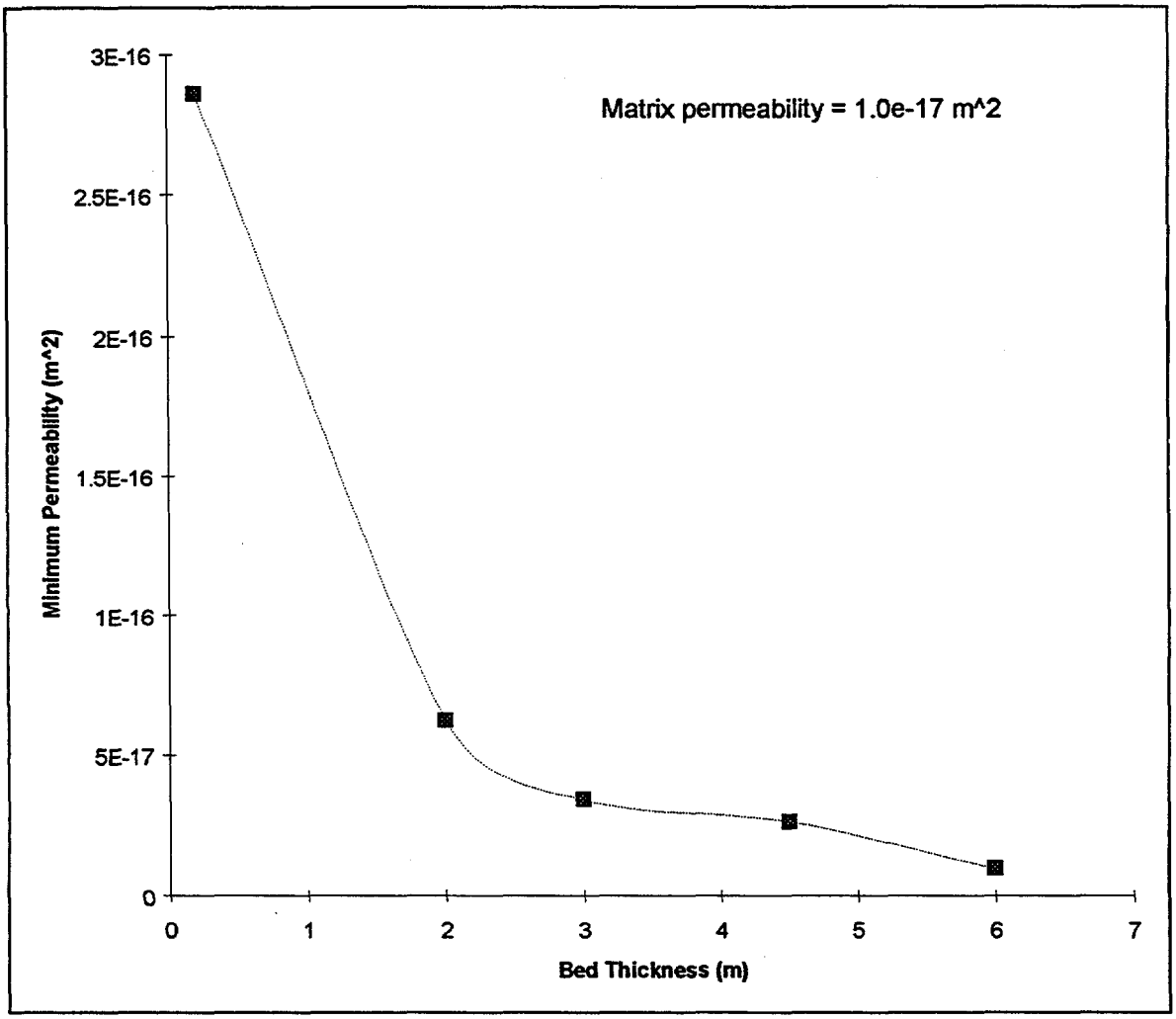

Figure 6.7. Bed thickness versus minimum horizontal permeability, k_y. For increasing bed thickness the maximum permeability approaches matrix permeability, and fractures will only affect the reservoir permeability in the main fracture direction.

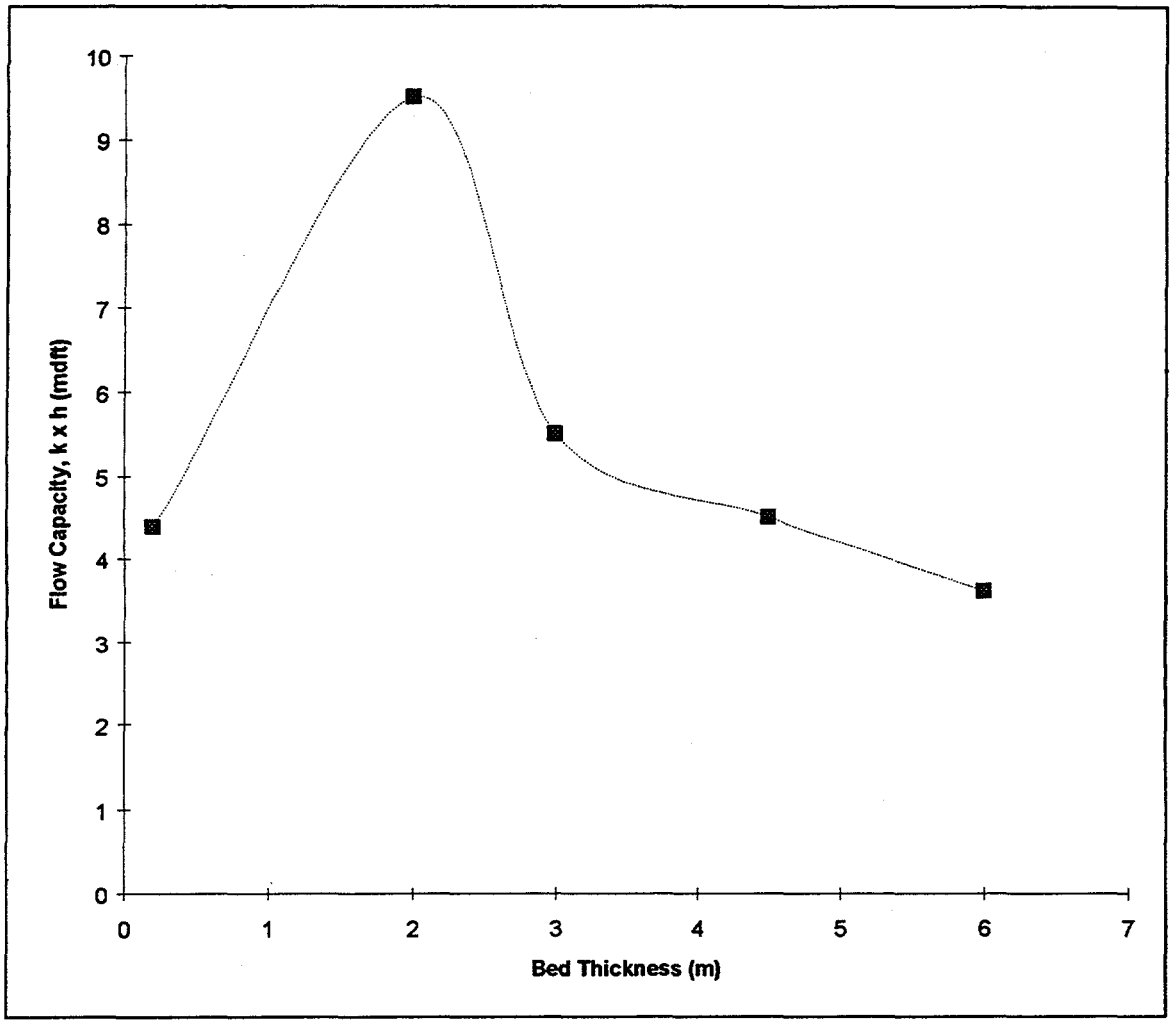

Figure 6.8. Bed thickness versus flow capacity.

6.3 Influence of Bed Thickness on Fracture Porosity and Storage Capacity

The outcrop fracture-network maps clearly show that the fracture intensity decreases with increasing bed thickness and that there are fewer and longer fractures per reservoir area and volume as the bed thickness increases. This change in the spatial distribution of fractures also affects the fracture porosity that can be calculated from Oda's model. The fracture porosity provides an estimate of the fracture intensity within a given reservoir volume. Figure 6.9 shows that the calculated fracture porosity decreases with increasing bed thickness. Note that the fracture porosity is very low for all cases decreasing from 0.02% for a bed thickness of 0.2 m to 0.0007 % for a bed thickness of about 6 m. Matrix porosity is assumed to be 14 % for the model calculations. Although the fracture porosity is very low and decreases with increasing bed thickness, the fracture porosity is always very effective porosity and directly contributes to the bulk permeability of the reservoir.

Storage capacity of an equivalent reservoir volume is a function of the total porosity (fracture and matrix porosity). For the Frontier sandstone, matrix porosity controls storage capacity. Accordingly, storage capacity increases linearly with bed thickness (Figure 6.10).

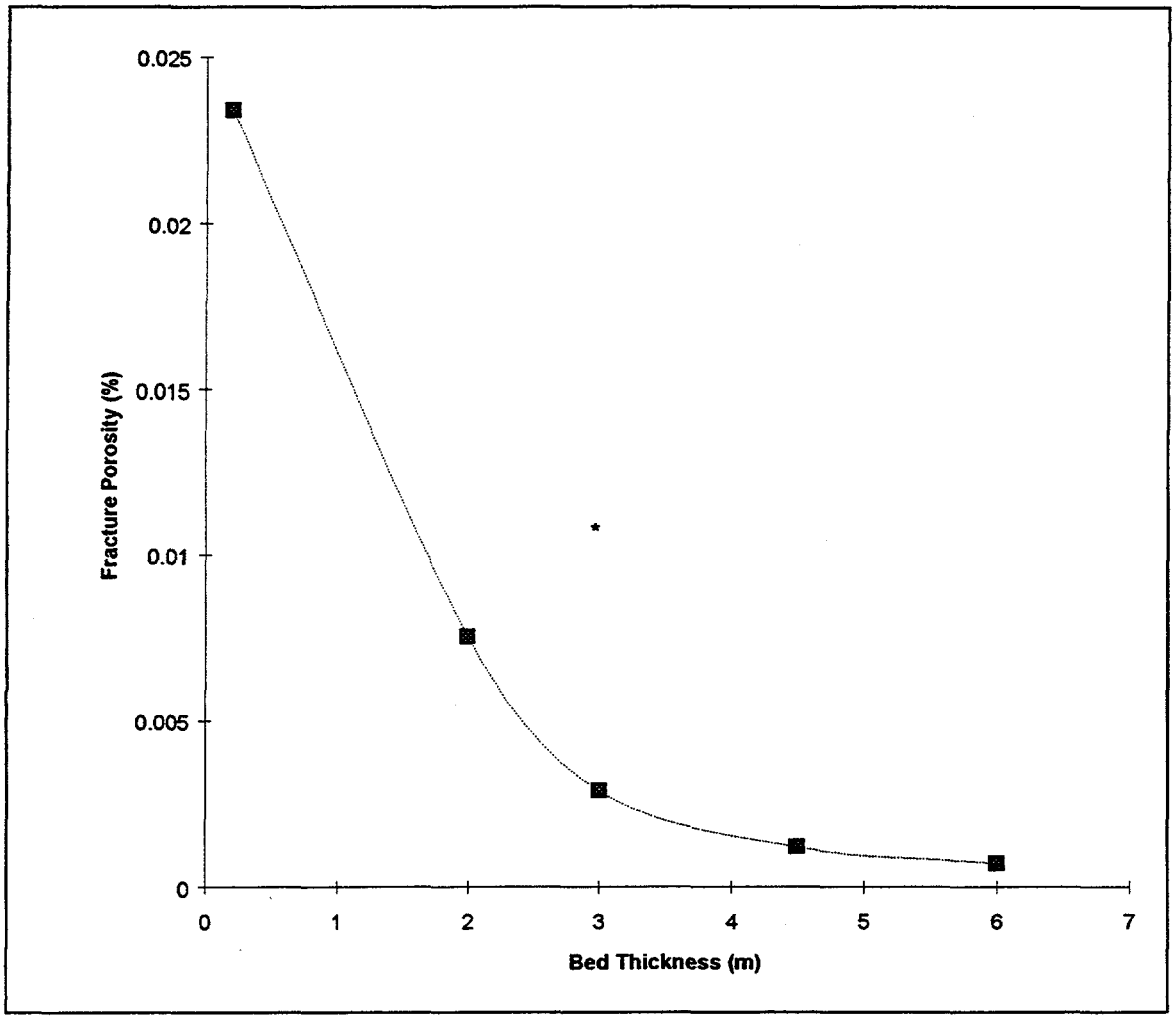

Figure 6.9. Plot of bed thickness versus fracture porosity (%). The small values for fracture porosity do not affect the reservoir storage capacity.

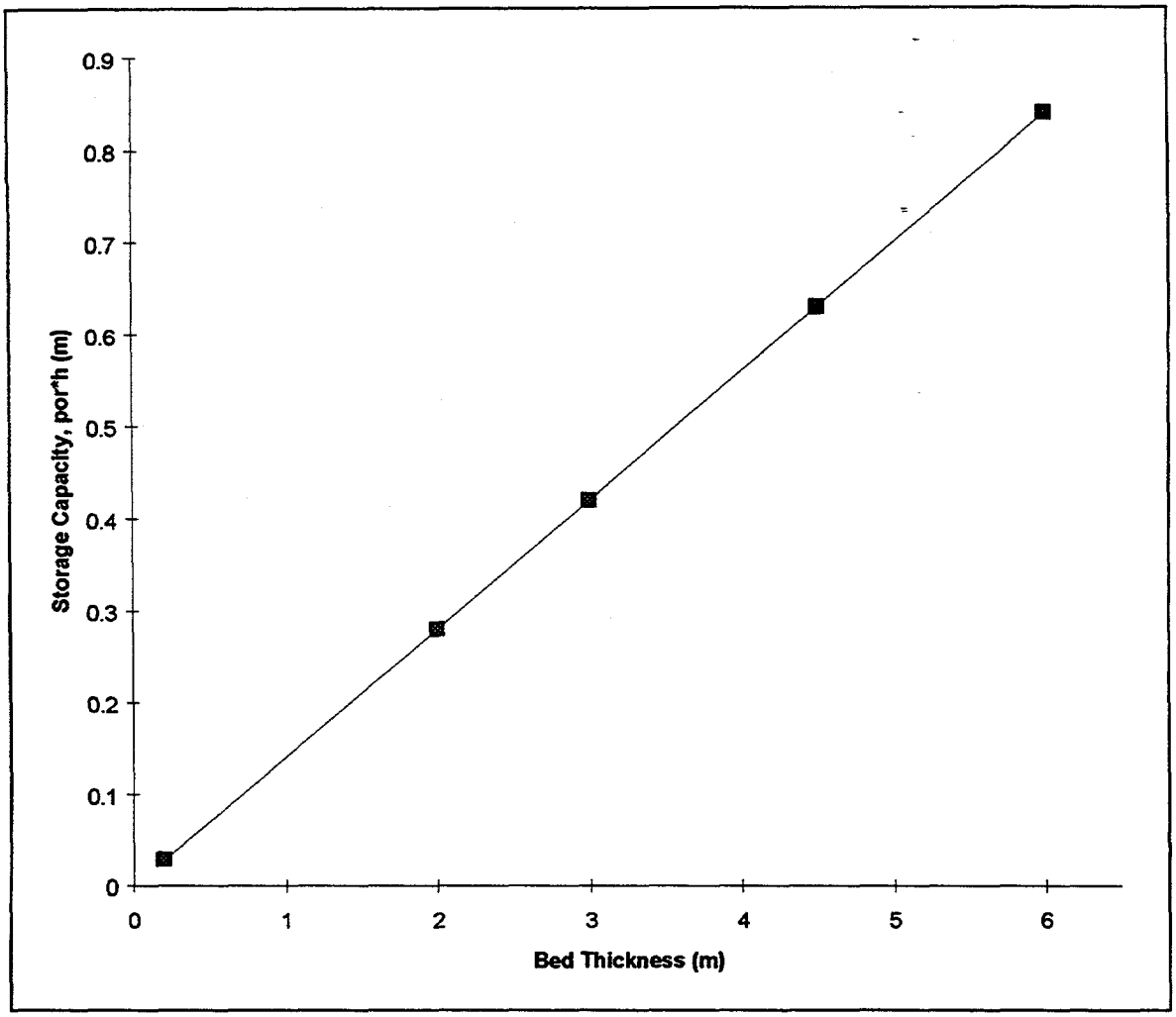

Figure 6.10. Bed thickness versus storage capacity. Storage capacity is only a function of matrix porosity, we therefore see a linearly increasing storage capacity for increasing bed thickness.

6.4 Reservoir Model Permeability

Modeled permeability in a reservoir simulation is very sensitive to fracture parameters, more specifically to the permeability anisotropy imposed on the matrix by the fracture system. In chapter five the tensor model was introduced as an approach to calculate permeability of regional fractures. A dual porosity sheet model can also be used. In Figure 6.11 the tensor model was compared to the sheet model (Reiss, 1980). The sheet model calculates the effective reservoir permeability based on a fixed, uniform geometry given by constant fracture spacing, constant aperture width, and thoroughgoing fractures. The tensor model is more flexible in its fracture modeling. Fractures are modeled with non-uniform geometry and variable intensity for a given area. The fracture spacing for the tensor model are taken from Figure 4.8.

The two models show significant differences in the calculated permeability. The tensor model always calculates a lower permeability, because fractures in the tensor model are laterally discontinuous whereas the sheet model they are modeled has continuous fractures. The two models have differences of nearly 60 % for bed-thickness greater than 3 m (Figure 6.13).

We believe the tensor model provides a better estimate of reservoir permeability, because this model takes into account the discontinuous nature of the fracture network. In the next chapter the calculated permeabilities will be applied as input in reservoir simulation to predict response of analogous gas reservoirs.

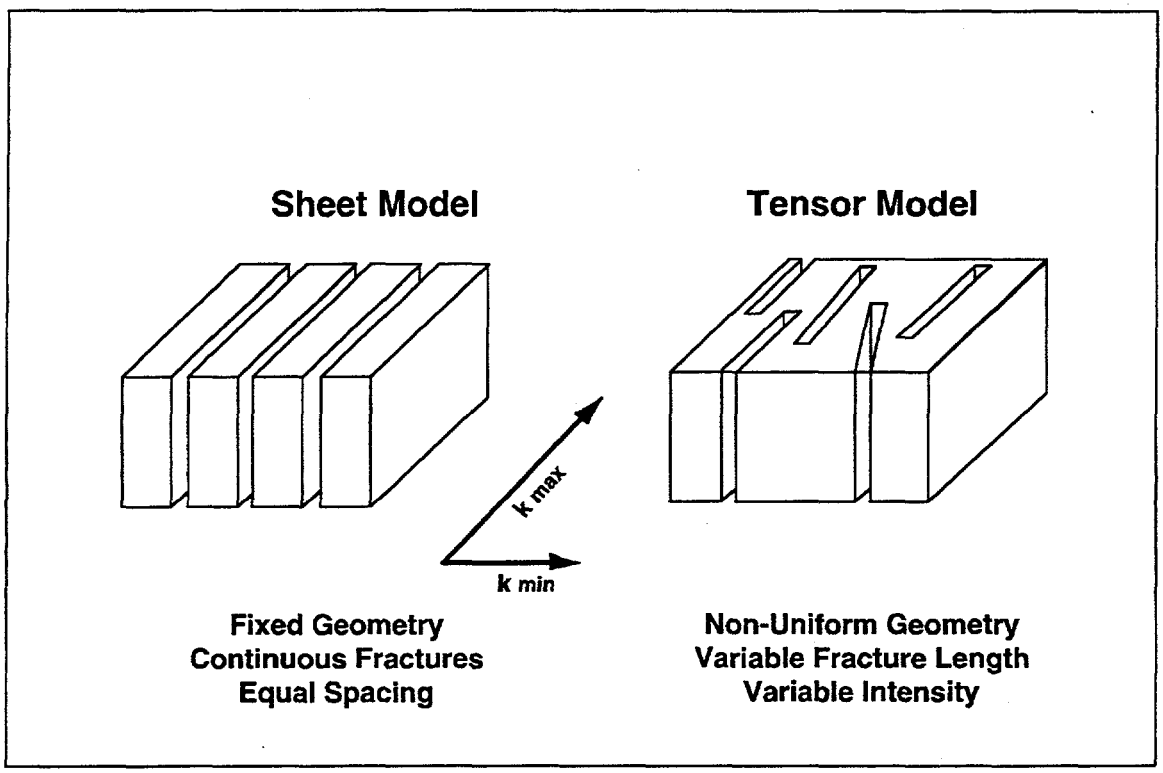

Figure 6.11. Tensor versus sheet model. The sheet model describes fractures of fixed geometry with continuous and equal spacing. The tensor approach models fractures with non-uniform geometry having variation in length, orientation and intensity.

Table 6.2. Comparison of maximum horizontal permeability determined by tensor and sheet model.

Bed thickness [m]	**Tensor model** [10^{-15} m^2]	**Sheet model** [10^{-15} m^2]
0.2	154.0	179.8
2	33.6	53.94
3	8.77	21.58
4.5	3.34	9.81
6	3.07	6.74

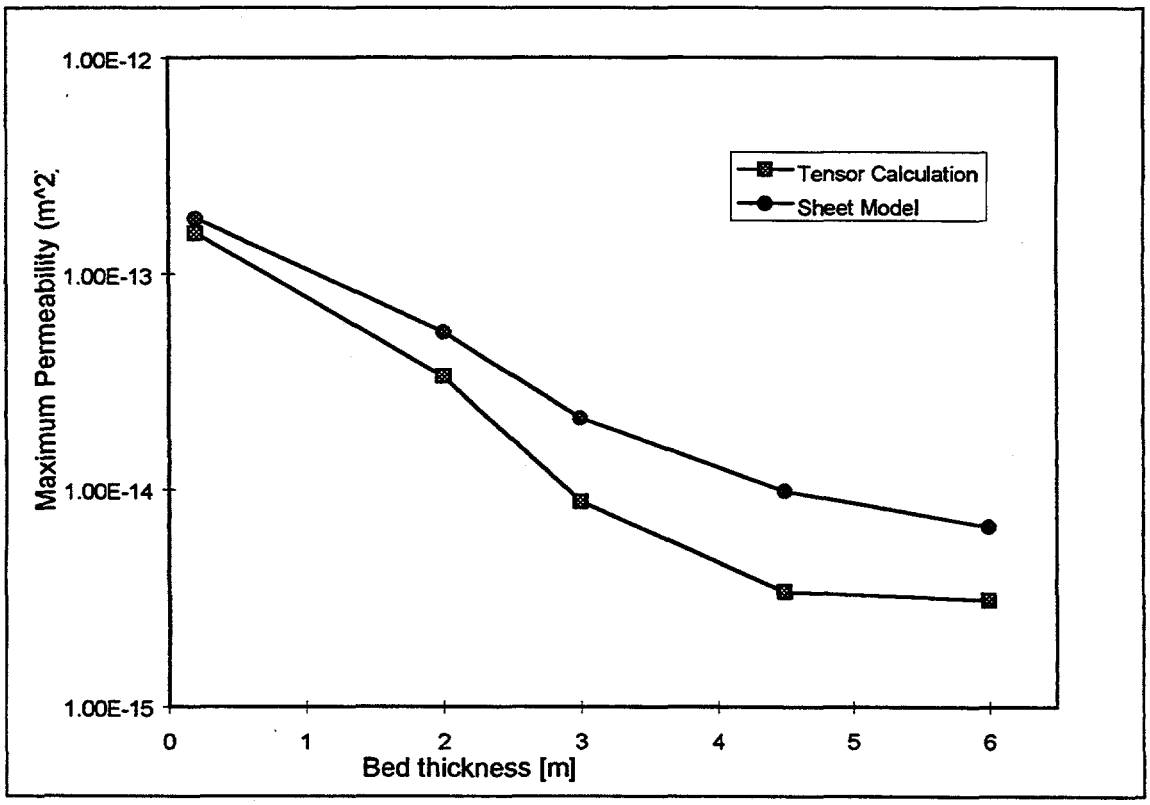

Figure 6.12. Comparison of calculated maximum horizontal permeability for tensor and sheet models. The tensor model always calculates a lower permeability, because fractures in the tensor model are not continuous, whereas they are modeled as continuous fractures in the sheet model.

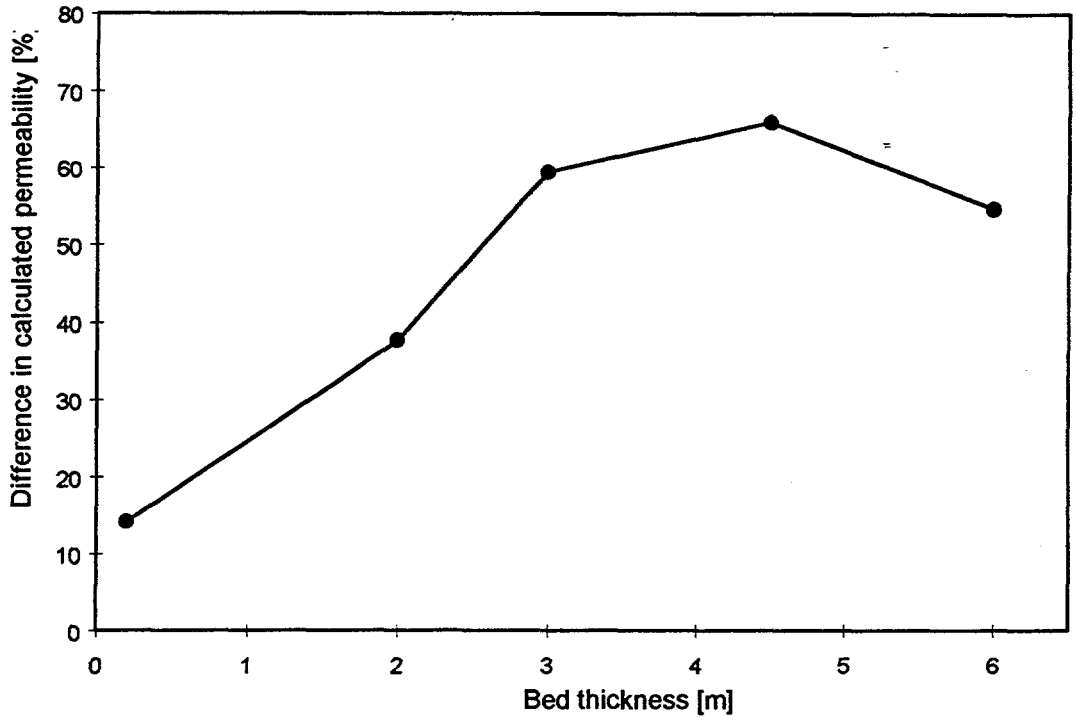

Figure 6.13. Percent difference between the tensor and sheet models for calculated maximum horizontal permeability as a function of bed thickness. With increasing bed thickness the difference in calculated permeability increases.

7. Reservoir Simulation

A single porosity, single permeability model is used to simulate fluid flow in analogous subsurface reservoirs that correspond to the fracture networks and bed thicknesses at four of the five outcrop locations. The 0.2 m bed thickness is not included because the storage capacity is to small to make this represent a real reservoir. The single porosity model can be used in this study instead of a dual porosity model because the method used to calculate the bulk permeability tensor has replaced the fractured rock mass by an unfractured rock mass which behaves equivalently, in the sense of flow rate and pressure gradient, to the original fractured medium. As previously discussed, this approach is compatible with the dual continuum concept proposed by Barenblatt (1960).

Other reasons for choosing the single model were:

1. Only one fluid phase, since the reservoirs are mainly gas producers.
2. Since only one phase is simulated, the more advanced modeling of gravity drainage and imbibition that a dual model can provide is not needed.

3. Lack of horizontal continuity and the complexity of the fracture network makes the sugar cube model inappropriate.
4. A dual model would only model flow from a matrix block to a fracture, and then from fracture to wellbore. It would not model cross-flow, that is flow from a matrix block crossing a fracture to flow into a new matrix block.

The single well, reservoir simulator "Well Performance Model" is used for the simulation. The code was provided by Phillips Petroleum Company.

7.1 Reservoir Model

The reservoir model is a 1.3 km^2 rectangular area (320 acres). The vertical depth to the top of the simulated layer is 3,350 m with an initial reservoir pressure of 72.4 Mpa (10,500 psi). Gas is the simulated fluid, with a density of 0.65 relative to air (air equals 1.0). The formation porosity is 14 % and matrix permeability is 1×10^{-17} (10 μd), which are average values for the Frontier sandstone. The reservoir has a 2 % irreducible water saturation. Maximum and minimum horizontal permeability varies with bed thicknesses and the values used for these parameters for the four cases, based on outcrop data, are given in Table 6.1.

Simulations of reservoir depletion were conducted for each of the four reservoir models to compare predicted gas production from vertical, hydraulically fractured wells to horizontal wells. Figure 7.1 shows the well completions and the expected drainage patterns in the reservoir model. The vertical well is placed in the center of the drainage rectangle and is completed through the entire vertical height of the reservoir bed. The well is stimulated with a vertical hydraulic fracture that is parallel to the regional natural fracture trend. It is assumed that the hydraulic fracture propagates parallel to the regional fracture trend, which is usually in the direction of the local maximum horizontal stress direction. The hydraulic fracture has a half-length of 170 m and has finite conductivity. The horizontal well is drilled perpendicular to the regional fracture trend and maximum permeability direction. Four different lengths of the completed section of the horizontal well are simulated. The lengths are full (1/1), 2/3, 1/2, and 1/3 the length of 320 acre rectangular drainage area.

The 20 cases were all set to produce at a target rate of 2000 MSCFD. Due to effects of a stress-sensitive matrix and natural fracture permeability, minimum wellbore pressure is 27.6 MPa. The production is ran over a 10 year period to see how long the wells are able to maintain this target gas rate (Figure 7.2). The cutoff rate is set to 400 MSCFD, and the cumulative production when this rate is reached is shown in Figure 7.3.

7.2 Simulation Results

The results show that the time a vertical well can maintain a target rate of 2000 MSCFD is less than one year for bed thicknesses of 2 to 6 m (Figure 7.2). The relationship between flow capacity and storage capacity is the cause for the small variation in time with changes in bed thickness. This result explains the conclusions by Moslow and Tillman (1984) that there

appeared to be no correlation between thickness of reservoir facies and net production for vertical wells in the Moxa arch area.

For horizontal wells, the time to maintain a target rate of 2000 MSCFD increases with increasing length of the completed well for a given bed thickness. Horizontal wells maintain the target rate for production for a longer time than a vertical well. For example, the time on target rate for production of a horizontal well extending half the reservoir length in a 3 m thick reservoir is more than five times greater than that of a vertical well.

Figure 7.3 shows the effect of completion on cumulative production. The vertical well is sensitive to the high initial rate, but still has a fairly high cumulative production. However, a horizontal well, extending half the reservoir length in the 6 m thick reservoir, has a cumulative production that is more than 50% greater than the vertical well. Longer horizontal wells are required for the same cumulative production with decreasing bed thickness.

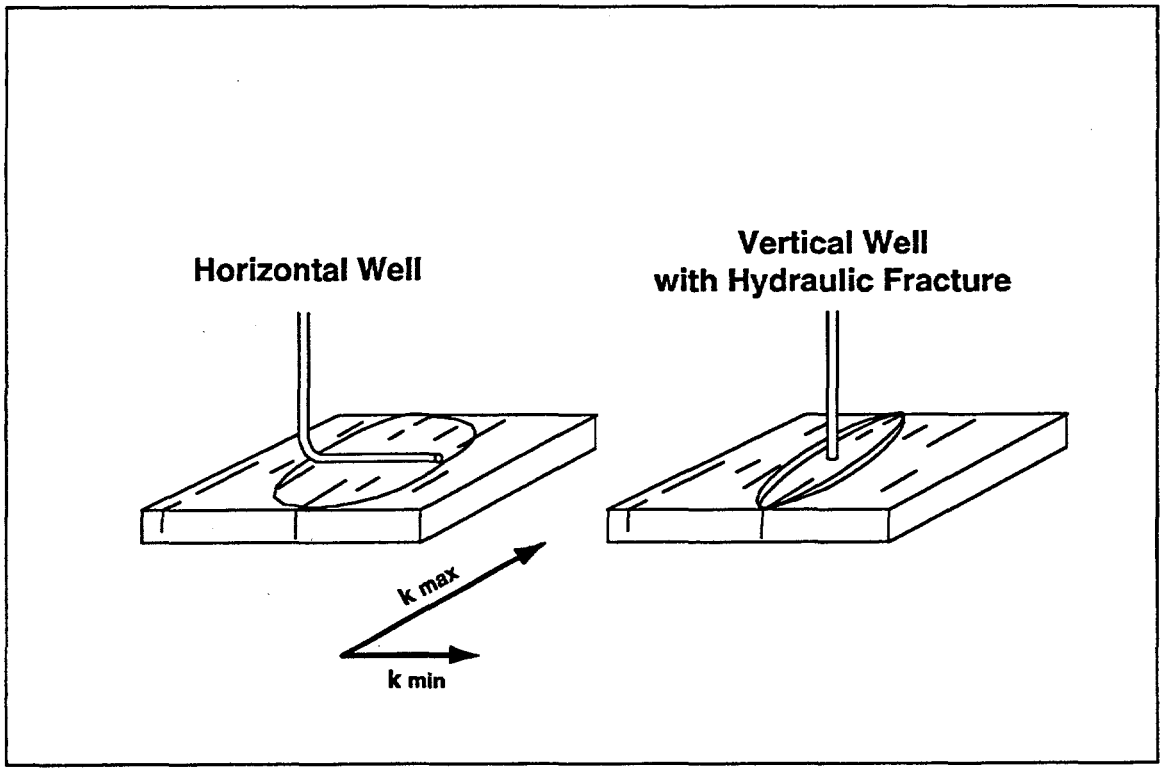

Figure 7.1 Comparison of drainage patterns for a horizontal well versus a vertical well with a hydraulic fracture. The vertical well is stimulated with a hydraulic fracture that parallels the regional fracture trend, whereas the horizontal well is drilled perpendicular to the fracture trend.

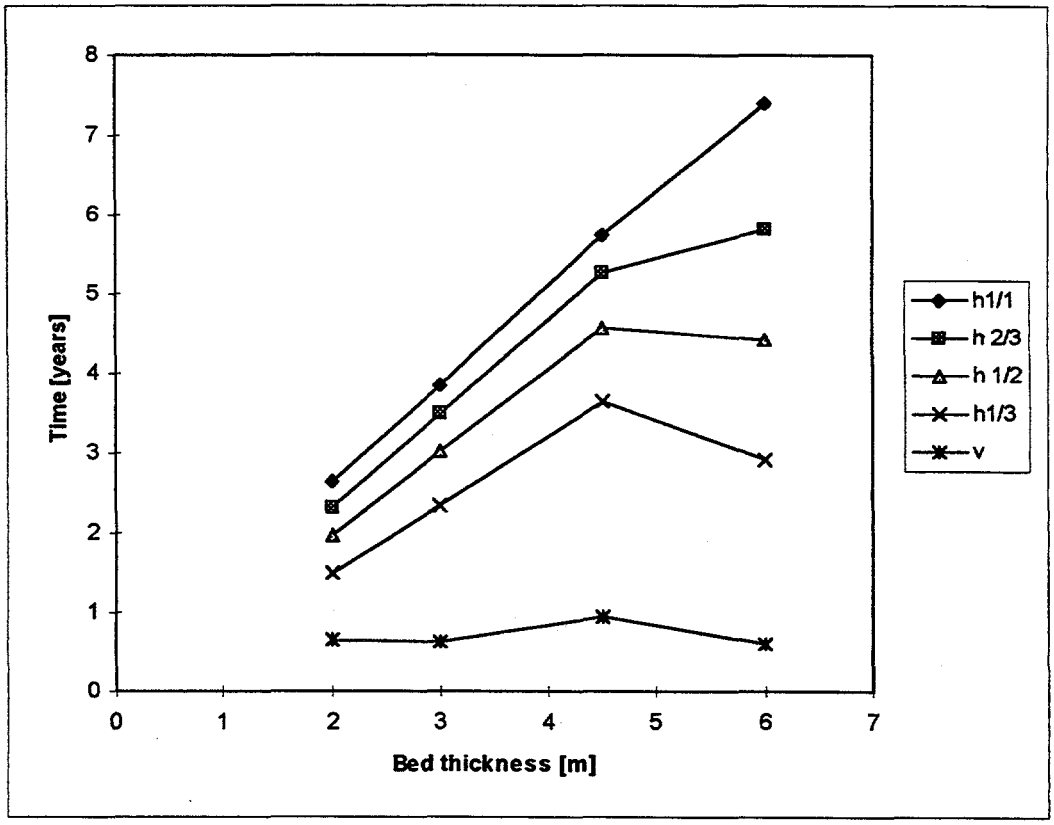

Figure 7.2. Time on target rate of 2000 MSCFD versus bed thickness for vertical well and horizontal wells of different lengths.

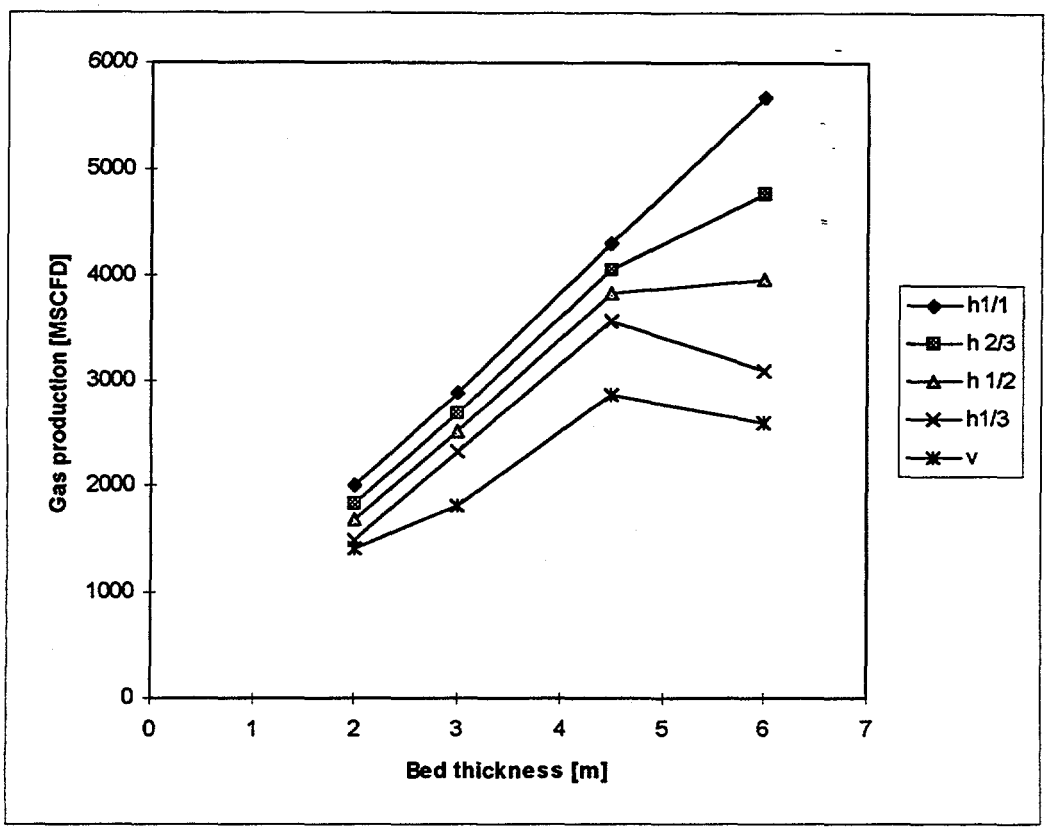

Figure 7.3. Cumulative production after 10 years versus bed thickness for vertical well and horizontal wells of different lengths.

8. Discussion

Significant gas reserves are present in low-permeability sandstones of the Frontier Formation in the greater Green River Basin, Wyoming. Successful exploitation of these reservoirs requires understanding the characteristics and fluid-flow response of the regional natural fracture system that controls productivity.

In this study, fracture characteristics were obtained from outcrops of Frontier sandstones which had different bed thicknesses at five locations in the basin. Regional fracture characteristics (orientation, length, and spatial distribution) obtained from the five outcrop fracture-network maps were combined with an assumed fracture aperture and matrix permeability data to compute an anisotropic permeability tensor (magnitude and direction) corresponding to analogous Frontier sandstone fracture systems in the subsurface, using Oda's permeability tensor method and Bruhn's computer program.

8.1 Fracture Characterization

The fracture network maps show that regional fractures are an unidirectional set of extension fractures that are oriented normal to bedding. These fractures are not laterally

continuous at the scale of the outcrop and do not have a consistent and equal spacing. In general there are fewer and longer fractures per unit area as the bed thickness increases. This change in the spatial distribution of fractures directly affects the calculated bulk permeability tensor of an equivalent reservoir volume in the subsurface. Model calculations show that the maximum and minimum horizontal permeability are controlled by fracture intensity and decrease with increasing bed thickness. The direction of maximum permeability is parallel to the regional fracture trend.

Oda's permeability tensor model for fractured rock has several advantages. The model calculates the permeability from the orientation, length, aperture, and spatial distribution of the fracture network in a representative volume, and honors the geologic characterization of the fracture network. The model directly calculates the orientation and magnitude of the horizontal permeability anisotropy from the total natural fracture population and is not limited to a continuous parallel set of fractures with uniform and equal fracture spacing as in the conventional dual-porosity models.

Oda's model is limited in application to predicting fluid-flow in the subsurface, because information on the horizontal spatial distribution and length of fractures cannot be obtained in the subsurface. However, sufficiently detailed fracture characterization, based on field outcrops as presented in this study, can provide a means to extrapolate surface fracture data to the subsurface. Fracture data from cores and logs would constrain this data and provide more realistic fracture characterization and fluid-flow model.

Another limiting factor for the model is the proper value to use for fracture aperture, which controls hydraulic conductivity. A constant aperture of 0.1 mm is assumed in this study for all fractures, independent of length. This parameter has the highest degree of uncertainty in the present model analysis, whereas orientation, length, and spatial distribution are known from the fracture network maps. Information on fracture aperture may be obtained from core studies and log analyses, but even this value is suspect and may not be representative of the hydraulic aperture in the subsurface reservoir at reservoir stress conditions. Fracture aperture may be the limiting factor in the model's application to reservoir analysis. However, fracture aperture could be better estimated from well tests or production tests by using the outcrop fracture maps to constrain other fracture data in the analysis of these tests.

8.2 Reservoir Simulation

The relationships between fracture intensity, bed thickness, and the calculated fluid-flow properties were used in a reservoir simulation study to make a comparison between 1) the predicted gas production from vertical, hydraulically fractured wells, and 2) horizontal wells that are drilled perpendicular to the regional fracture trend and maximum permeability direction. A single-porosity, single-permeability model was used in this simulation because the calculated bulk permeability tensor is equivalent to a dual porosity system.

The simulation results show that gas production at high rates can be maintained for a longer time from horizontal wells than from vertical, hydraulically-fractured wells. Cumulative

gas production is also greater from horizontal wells than from vertical wells. Longer horizontal wells are required for the same cumulative production with decreasing bed thickness. In these simulations a minimum horizontal well length of 1/3 the length of reservoir drainage area always has higher production than a vertical well.

The higher productivity in horizontal wells is related to the reservoir permeability anisotropy. In the horizontal wells, drainage is set perpendicular to the maximum horizontal permeability and more effectively drains the reservoir. In the vertical wells, however, the hydraulic fracture parallels the regional fractures and maximum permeability trend and therefore only increases the elliptical shape of the drainage area (Figure 7.1).

A limitation to using a single porosity, single permeability model in a fractured reservoir is that the diffusion time between matrix and fracture cannot be modeled. The diffusion time increases as the contrast between matrix and fracture permeability increases. Accordingly, for tight gas reservoirs it is suggested that long term production decline curves rather than short term well tests should be used to validate the reservoir model.

Fracture characterization and simulation of Frontier sandstone reservoirs in this study suggest that these tight-gas reservoirs may be optimum targets for horizontal drilling. However, the reservoir management decision to drill horizontal wells, that are more expensive than hydraulically fracture vertical wells, to produce these reservoirs must be based on economics. Large scale production tests are needed before this decision can be made.

9. Conclusions

As a result of this study the following general conclusions can be drawn:
Fracture characterization has been done at four selected outcrops of the Frontier sandstone by constructing detailed fracture maps. The maps provided information on fracture orientation, lengths, and spatial distribution.

Outcrop studies clearly demonstrate that regional fractures in the Frontier sandstone have unequal fracture spacing, varying lengths, and are not laterally continuous at the scale of the outcrop.

Bed thickness directly affects the spatial distribution of these fractures. Fewer and longer fractures occur per unit area as bed thickness increases.

Fracture data were combined with matrix permeability data to compute an anisotropic permeability tensor (magnitude and direction) corresponding to an equivalent fracture system in the subsurface for different reservoir bed thickness.

Maximum and minimum horizontal permeabilities are controlled by fracture intensity and decrease with increasing bed thickness.

Reservoir simulation using outcrop fracture data and the calculated permeability tensors shows no correlation between bed thickness and rate dependent production for vertical wells. This result is in agreement with field observations.

Horizontal wells drilled perpendicular to the maximum permeability direction should be able to maintain a high target gas-production rate for a longer time and should have higher cumulative production than vertical hydraulically-fractured wells. Longer horizontal wells are required for the same cumulative production with decreasing bed thickness.

10. References

Angelier, J., Souffache, B., Barrier, E., Bergerat, F., Bouaziz, S., Bouroz, C., Creuzat, G., Ouali, J., and Tricart, P., 1989; "Distribution de Joints dans un Banc Rocheux: loi Theorique et espacements," Comptes Rendeus, Academie des Sciences de Paris, Vol. 309, p. 2119-2125.

Barenblatt, G. I., Zheltov, Iu. P., and Kochina, I. N.; "Basic Concepts in the Theory of Seepage of Homogenous Liquids in Fissured Rocks (Strata)," Soviet J. Appl. Math.. Mech., 1960, 24(5), 1286-1303.

Barlow, J. A. Jr., Doelger M. J., Mullen, D. M., and Barlow & Haun, Inc., 1993; *Atlas of Major Rocky Mountain Gas Reservoirs*, New Mexico Bureau of Mines and Mineral Resources, Socorro, New Mexico, p. 33.

Bear, J., 1972; *Dynamic of fluids in porous media*, New York: Elsevier.

Bering, D., Bruhn, R. L., and Magnus, C., 1994; "Modeling of fracture systems & fluid flow from analogue field studies," EAPG/AAPG Special Conference on Chalk, Copenhagen, Denmark.

Bruhn, R. L., 1994; "Two Dimensional Fracture Network Analysis," MATLAB script files, Department of Geology and Geophysics, University of Utah with support of the Norwegian Petroleum Directorate, Stavanger, Norway.

De Chadenedes, J. F., 1975; "Frontier Deltas of the Western Green River Basin, Wyoming," Deep Drilling Frontiers of the Central Rocky Mountains, Rocky Mt. Assoc. Geologists Symposium, p. 149-157.

Doelger M. J., Mullen, D. M., and Barlow & Haun, Inc., 1993; *Atlas of Major Rocky Mountain Gas Reservoirs*, New Mexico Bureau of Mines and Mineral Resources, Socorro, New Mexico, p. 50-53.

Dutton, S. P., and Hamlin, H. S., 1991; "Geologic Controls on Reservoir Properties of Frontier Formation Low-Permeability Gas Reservoirs, Moxa Arch, Wyoming," Society of Petroleum Engineers, SPE Paper 21851, p. 479-488.

Elkins, L. F., and Skov, A. M., 1960; "Determination of Fracture Orientation from Pressure Interference Transactions," AIME 219, 301-304.

Gramberg, J., 1965; "Axial Cleavage Fracturing, a Significant Process in Mining and Geology," Engineering Geology, Vol. 1, P. 31-72.

Hamlin, H. S, 1991; "Stratigraphy and Depositional Systems of the Frontier Formation and their Controls on Reservoir Development, Moxa Arch, Southwestern Wyoming," Bureau of Economic Geology, The University of Texas at Austin, topical report prepared for the Gas Research Institute under contract No. 5082-211-0708, 44 pp. (Figure 2.3)

Hancock, P. L., Al Kadhi, A., and Sha'at, N. A., 1984; "Regional Joint Sets in the Arabian Platform as Indicators of Intraplate Processes," Tectonics, Vol. 3, p. 27-43.

Harris, J. F., Taylor, G. L., and Walper, J. L., 1960; "Relation of Deformational fractures in Sedimentary Rocks to Regional and Local Structures," AAPG Bulletin, Vol. 44, p. 1853-1873.

Harstad, H., 1995; *Characterization and Simulation of Naturally Fractured Frontier Sandstone, Green River Basin, Wyoming,* M.Sc. Thesis, New Mexico Institute of Mining and Technology, 86 p., May.

Hodgson, R. A., 1961; "Regional Study of Jointing in Comb Ridge-Navajo Mountain area, Arizona and Utah," AAPG Bulletin, Vol. 45, p 1-38.

Knight, W. C., 1902; " The Petroleum Fields of Wyoming," Eng. and Min. Journ., Vol. 73, p. 721.

Kulander, B. R., Barton, C. C., and Dean, S. L., 1979; *The Application of Fractography to Core and Outcrop Fracture Investigations*, Department of Energy, Morgantown Energy Technology Center, Report METC/SP-79/3, 174 p.

Ladeira, F. L. and Price, N. J., 1981; " Relationship Between Fracture Spacing and bed Thickness," Journal of Structural Geology 13, p. 179-183.

Law, B. E., Spencer, C. W., Charpentier, R. R., Crovelli, R. A., Mast, R. F., Dolton, G. L., and Wandrey, C. J., 1989; "Estimates of gas resources in overpressured low-permeability Cretaceous and Tertiary sandstone reservoirs, Greater Green River Basin, Wyoming, Colorado, and Utah," in Eisert, J. L. (ed.), Wyoming Geological Association 40th field Conference Guidebook, p. 39-61.

Long J. C. S., Remer, J. S., Wilson, C. R., and Witherspoon, P. A., 1982; "Porous Media Equivalents for Networks of Discontinuous Fractures," Wat. Resour. Res. 18, No. 3, p. 645-658.

Lorenz, J. C., 1995; "Stresses and fractures in the Frontier Formation, Green River Basin, predicted from basin-margin tectonic element interactions," Wyoming Geological Association, Field conference guidebook, p. 45-60.

Lorenz, J. C., and Finley, S. J., 1991; "Regional Fractures II: fracturing of Mesaverde Reservoirs in the Piceance Basin, Colorado," The American Association of Petroleum Geologists Bulletin, VOL. 75, No. 11, November 1991, p. 1738-1757.

Lorenz, J. C., and Finley, S. J., 1989; "Differences in Fracture Characteristics and Related Production: Mesaverde Formation, northwestern Colorado," SPE Formation Evaluation, VOL. 4, p. 11-16

Lorenz, J. C., and Hill, R. E., 1991; "Subsurface Fracture Spacing: Comparison of Inferences from Slant/Horizontal Core and Vertical Core in Mesaverde Reservoirs," SPE paper 21877, Joint Rocky Mountain Section Meeting and Low-Permeability Reservoir Symposium, p. 705-716.

Lorenz, J. C., and Laubach, S. E., 1994; *Description and Interpretation of Natural Fracture Patterns in Sandstones of the Frontier Formation Along the Hogsback, Southwestern Wyoming*, Gas Research Institute, Topical report, GRI-94/0020.

Lorenz, J. C., Teufel, L. W., and Warpinski, N. R., 1991; "Regional Fractures I: A mechanism for the Formation of Regional Fractures at Depth in Flat-Lying Reservoirs," The American Association of Petroleum Geologists Bulletin, VOL. 75, No. 11, p. 1714-1737.

Mallory, W. W., 1977; "Oil and Gas from Fractured Shale Reservoirs in Colorado and northwest New Mexico," Rocky Mountain Association of Geologists Special Publication 1, 38 p.

Moslow, T. F., and Tillman, R. W., 1989; "Characterization, Distribution of Frontier Formation Reservoir Facies of Wyoming Fields," Oil and Gas Journal, May 29.

Moslow, T. F., and Tillman, R. W., 1984; "Sedimentary Facies and Reservoir Characterization of Frontier Formation Sandstones, Southwestern Wyoming," American Association of Petroleum Geologists, Studies in Geology 24, p. 271-295.

Mullen, D. M., and Barlow & Haun, Inc., 1993; *Atlas of Major Rocky Mountain Gas Reservoirs, New Mexico Bureau of Mines and Mineral Resources*, Socorro, New Mexico, p. 52.

Muskat, M., 1949; *Physical Principles of Oil Production*, New York McGraw-Hill, 922 p.

Myers, R. C., 1977; "Stratigraphy of the Frontier Formation (Upper Cretaceous), Kemmerer Area, Lincoln County, Wyoming," Twenty-Ninth Annual Field Conference, Wyoming Geological Association Guidebook.

Nelson, R. A., 1985; *Geologic Analysis of Naturally Fractured Reservoirs*, Houston, Gulf Publishing, p 320.

Nelson, R. A., 1982; "An Approach to Evaluating Fractured Reservoirs," Journal of Petroleum Technology, September.

Nickelsen, R. P. and Hough, V. N. D., 1967; "Jointing in the Appalachian Plateau of Pennsylvania," Geological Society of America Bulletin, VOL. 14, p. 609-630.

Obradovich, J. D. and Cobban, W. A., 1975; "A Time Scale for the Late Cretaceous of the Western Interior of North America," Geol. Assoc. Canada Sp. Paper No. 13, p. 31-54.

Oda, M., 1986; "An Equivalent Continuum Model for Coupled Stress and Fluid Flow Analysis in Jointed Rock Masses," Water Resources Research, Vol. 22, No. 13, p. 1845-1856, December.

Oda, M., 1985; "Permeability Tensor for Discontinuous Rock Masses," Geotechnique 35, No. 4, 483-495.

Parker, J. M., 1942; "Regional Systematic Jointing is slightly Deformed Sedimentary Rocks," Geological Society of America Bulletin, Vol. 53, p. 381-408.

Parsons, R. W., 1966.; "Permeability of Idealized Rock," SPE. Jour., June,. p. 126-136.

Petroleum Information, 1976; "Monthly Production Report of Oil and Gas in Wyoming," October.

Pollard, D. D., and Aydin, A., 1988; "Progress in understanding jointing over the past century," Geological Society of America Bulletin, Vol. 100, p. 1181-1204.

Reiss L. H. 1980; *The Reservoir Engineering Aspects of Fractured Formations*, Gulf Publishing Company

Scheidegger, A. E., 1957; *The Physics of Flow through Porous Media*, University of Toronto Press.

Scotia Group, 1993; *Reserves in western basins part I: Greater Green River Basin, Report to the US Department of Energy*, Office of Fossil Energy, Morgantown Energy Technology Center, DOE/MC/28130-3534 (DE94000060), 146 p. plus 3 appendices.

Segall, P., and Pollard, D. D., 1983; "Joint Formation in Granitic Rocks of the Sierra Nevada," Geological Society of America Bulletin, Vol.94, p. 563-575.

Stearns, D. W., and Friedman, M., 1972; "Reservoirs in Fractured Rock," in R. E. King, ed., Stratigraphic Oil and Gas Fields-Classification, Exploration Methods, and Case Histories, AAPG Memoir 16, p. 82-106.

Veatch, A. C., 1906; "Coal and Oil in Southern Uinta County, Wyoming," US Geological Survey Bulletin 285, p. 331-353.

Veatch, A. C., 1907; "Geology and Geography of a Portion of Southwestern Wyoming," US Geological Survey Prof. Paper 56, 178 p.

Verbeek, E. r., and Grout, M. A., 1984; "Fracture Studies in Cretaceous and Paleocene Strata in and around the Piceance Basin, Colorado," preliminary results and their bearing on a Fracture-Controlled Natural Gas Reservoir at the MWX site: USGS Open File Report 84-156, 30 p.

External Distribution:

US Dept. of Energy (10)
P. O. Box 1398
Bartlesville, OK 74005
Tom Wesson (5)
R. Lemmon (5)

US Dept. of Energy (10)
Collins Ferry Rd.
Morgantown, WV 26505
K.H. Frohne (5)
T. Mrose (5)

Gas Research Institute (3)
8600 West Bryn Mawr Dr.
Chicago, IL 60631
S. Wolhart
T. Fate
R. Parker

NM Tech, PNGE Dept. (30)
Socorro, NM 87801
H. Harstad (25)
L. Teufel (5)

Meridian Oil (2)
P. O. Box 3209
Englewood, CO 80155-3209
J. Minelli
W. Whiteman

Meridian Oil (2)
P. O. Box 4289
Farmington, NM 87499-4289
W. Babcock
B. Ault

Chevron USA Production Co. (2)
P. O. Box 1635
Houston, TX 77251
Kirby Aslesan
Kent Bowker

Parker and Parsley (2)
PO Box 3178
Midland, TX 79072-3178
T. Sheffield
P. McDonald

Connie Jump
Enron Oil and Gas Co
1625 Broadway, Suite 1300
Denver, CO 80202

Shell Western E&P Inc (3)
P. O. Box 4252
Houston, TX 77079
R. Rozen
M. Picha
B. Cain

Vastar Resources Inc (2)
15375 Memorial Drive
Houston, TX 77079
S. Parks
M. Gale

Lee Robinson
Vessels Oil and Gas Co.
Suite 2000, Prudential Plaza
1050 17th St
Denver, CO 80265

Tom Hoak
Advanced Reosurces Int'l.
165 S. Union Blvd., Suite 816
Lakewood, CO 80228

Greg Francis
Celsius Energy Co.
1331 17th St, Suite 800
Denver, CO 80202

Amoco Production Co. (4)
1670 Broadway
P. O. Box 800
Denver, CO 80201
R. Billingsley
L. Evans
D. Pivnik
H. Terbest

Pat McLellan
Advanced Geotechnology Inc.
Suite 800
333 5th Ave. SW
Calgary, Alberta T2P 3B6
CANADA

Union Pacific Resources (3)
P. O. Box 7
Fort Worth, TX 76101-0007
L. Krystinik
R. Mead
F. Lim

Terry Barrett
Barrett Energy
1125 17th St, Suite 2100
Denver, CO 80202

Tom Dunn
Institute of Energy Resources
University of Wyoming
P. O. Box 4968
Laramie, WY 82071

C. Dennis Irwin
220 Cimmaron Way
Boulder, CO 80303

Ron Johnson
USGS, MS 939
Denver Federal Center
Denver, CO 80202

D. Weinberg
INEL
P. O. Box 1625
Idaho Falls, ID 83415-3710

Jan Holthe
Saga Petroleum
PO. Box 490
1301 Sandvika
NORWAY

S"ren Priisholm
M'RSK OLIE OG GAS
50 Espelanden
DK-1263 Copenhagen
DENMARK

Chris Dart
Z & S Geology
Sverdrupsgate 23
4007 Stavanger
NORWAY

Trond Unneland
Statoil
PO Box 620
4001 Stavanger
NORWAY

Statoil - Research Center (4)
Postuttak
7004 Trondheim
NORWAY
Haakon G. Rueslaatten
Paal-Eric Oren
Chris Townsend
William England

Tor Hemmingsen (2)
Rogaland Research
PO Box 2503 Ullandhaug
4004 Stavanger
NORWAY

Rasmus Risnes
Rogaland University Center
P. O. Box 2557
Ullandhaug
4001 Stavanger
NORWAY

Phillips Petroleum (3)
PO Box 220
4056 Tananger
NORWAY
Hroar Hermansen
Steinar Edholm
Aly Anis Hamouda

Alan Khatib
RMOTC
907 N. Poplar, Suite 100
Casper, WY 82601

Internal Distribution:

5	MS0899	Technical Library, 4414
1	MS0706	D. A. Northrop, 6112
5	MS0705	J. C. Lorenz, 6114
1	MS0751	S. R. Brown, 6117
1	MS0751	J. T. Fredrich, 6117
1	MS0751	W. R. Wawersik, 6117
5	MS0751	File, 6117
1	MS9018	Central Technical Files, 8523-2
2	MS0619	Review & Approval Desk, 12630 For DOE/OSTI